A community-science approach identifies genetic variants associated with three color morphs in ball pythons (*Python regius*)

Autumn R. Brown[1], Kaylee Comai[1], Dominic Mannino[1], Haily McCullough[1], Yamini Donekal[1], Hunter C. Meyers[1], The BIO306 Consortium[1,2], Chiron W. Graves[1*], and Hannah S. Seidel[1*]

[1]Department of Biology, Eastern Michigan University, Ypsilanti, MI, USA

[2]The BIO306 Consortium comprises students in an undergraduate laboratory course at Eastern Michigan University who collected most of the data in this study. Students are listed under Acknowledgments.

*Correspondence: hseidel@emich.edu, cgraves6@emich.edu

Abstract

Color morphs in ball pythons (*Python regius*) provide a unique and largely untapped resource for understanding the genetics of coloration in reptiles. Here we use a community-science approach to investigate the genetics of three color morphs affecting production of the pigment melanin. These morphs—Albino, Lavender Albino, and Ultramel—show a loss of melanin in the skin and eyes, ranging from severe (Albino) to moderate (Lavender Albino) to mild (Ultramel). To identify genetic variants causing each morph, we recruited shed skins of pet ball pythons via social media, extracted DNA from the skins, and searched for putative loss-of-function variants in homologs of genes controlling melanin production in other vertebrates. We report that the Albino morph is associated with missense and non-coding variants in the gene *TYR*. The Lavender Albino morph is associated with a deletion in the gene *OCA2*. The Ultramel morph is associated with a missense variant and a putative deletion in the gene *TYRP1*. Our study is one of the first to identify genetic variants associated with color morphs in ball pythons and shows that pet samples recruited from the community can provide a resource for genetic studies in this species.

Introduction

Color patterns are distinctive and beautiful features of many animal species. Among the many functions of color are to camouflage animals to their surroundings, protect tissues from ultraviolet radiation, warn predators of poisons, and provide signals for mating and social communication (Cuthill et al., 2017). Color patterns have also been targeted by artificial selection to create novel and fanciful color patterns in pets and livestock (Cieslak et al., 2011).

Colors are produced through a combination of chemical pigments and physical structures (structural colors). Pigments absorb light, whereas structural colors are created when light is reflected by the nanoscale geometry of a tissue. Common pigments include brown-to-black melanin, present throughout the animal kingdom, and yellow-to-red carotenoids and pteridines, common in birds, reptiles, and lower vertebrates (Toews et al., 2017). Color-producing structures include ordered keratin matrices in bird feathers (Prum, 2006), chitin layers in butterfly wings (Ghiradella, 1985), and purine crystals in the skin of fish, amphibians, and reptiles (Bagnara et al., 1968; Saenko et al., 2013). These color-producing structures can produce a variety of colors, including iridescent colors, depending on the wavelengths of light they reflect (Kinoshita and Yoshioka, 2005).

The genetics and development of color patterns in vertebrates have been studied most extensively in mammals. Mammals largely rely on a single pigment (melanin), produced in the skin by a single type of cell (melanocyte) (Slominski et al., 2004). This system provides mammals with skin colors and hair colors ranging from black to reddish-brown, depending on the chemical structure of the melanin pigments (Meredith and Sarna, 2006).

Skin colors outside mammals are arguably more diverse and include bright colors of all hues. This increased complexity of colors is produced through a combination of structural colors and melanin and non-melanin pigments (Bagnara et al., 2007; Olsson et al., 2013; Shawkey and D'Alba, 2017) and relies on multiple types of specialized color-producing cells in the skin

(Bagnara and Matsumoto, 2008; Singh and Nüsslein-Volhard, 2015). Color cell development has been characterized to some extent in fish (Huang et al., 2021; Kimura et al., 2014; Nüsslein-Volhard and Singh, 2017), and genes controlling the use of non-melanin pigments have been identified in a few species of fish and birds (Cooke et al., 2017; Gazda et al., 2020; Kwon et al., 2021; Lopes et al., 2016; Mundy et al., 2016; Toomey et al., 2017; Zhang et al., 2021). The genetics and development of non-mammalian color patterns is less well understood in other vertebrates, particularly in reptiles (although see Garcia-Elfring et al., 2020; Guo et al., 2021; McLean et al., 2017; Ullate-Agote et al., 2020).

A unique resource for understanding the genetics of color patterns in reptiles is the ball python (*P. regius*). Ball pythons are native to sub-Saharan Africa, but have become common as pets in the United States (Bale, 2020). Wild ball pythons exhibit a mottled color pattern, consisting of brown-to-black melanin and red-to-yellow (non-melanin) pigments in the skin (Figure 1). Captive-bred ball pythons, by contrast, include many variants of the normal color pattern (Broghammer, 2019; Garcia-Elfring et al., 2020; Irizarry and Bryden, 2016; McCurley, 2005). These variants, referred to as ‘color morphs’, include animals having reduced melanin (e.g. Albino), increased melanin (e.g. Cinnamon), reduced red-to-yellow coloration (e.g. Axanthic), or complex changes in the placement of color patches on the skin (e.g. Spider, Clown, Genetic Stripe, and Enchi). Many color morphs are heritable and show simple dominant or recessive patterns of inheritance. These inheritance patterns are consistent with single-gene causality, but only a single genetic variant associated with a ball python color morph (Piebald) has been identified to date (Garcia-Elfring et al., 2020). Ball pythons therefore represent a tractable yet largely untapped resource for understanding the genetics of coloration in reptiles. An additional feature of ball pythons convenient for genetic studies is that DNA samples can be obtained non-invasively from shed skin (Burbrink and Castoe, 2011).

The goal of the current study was to perform proof-of-concept experiments to identify the genetic causes of three color morphs in ball pythons, using shed skins of pet ball pythons

recruited via social media. To keep the genetic analyses as simple as possible, we focused on three morphs for which candidate genes could be readily identified: Albino, Lavender Albino, and Ultramel. These morphs show a loss of brown-to-black coloration in the skin and eyes, characteristic of a defect in melanin production (Figure 1). These morphs are recessive and non-allelic (i.e. crosses between these morphs yield offspring with normal coloration), and their loss of melanin ranges from severe (Albino) to moderate (Lavender Albino) to mild (Ultramel). This range of phenotypes mirrors the range of phenotypes observed for loss-of-function variants in genes required for melanin production in other vertebrates (Table 1). This similarity provided a list of candidate genes that we predicted might harbor loss-of-function variants causing the Albino, Lavender Albino, and Ultramel color morphs in ball pythons. Our study demonstrates the feasibility of using community-sourced samples for genetic studies in ball pythons and lays the groundwork for future investigations of reptile-specific color patterns in this species.

Table 1. Loss-of-function phenotypes of melanogenesis genes across vertebrates.

Gene	Species in which putative loss-of-function variants have been described		Role of protein	Loss-of-function phenotype
TYR	Fish	Japanese carp (Liu et al., 2019), Japanese rice fish (Koga et al., 1999)	Rate-limiting enzyme in melanin synthesis pathway	Severe loss of melanin
	Frogs and snakes	Japanese wild frogs (three species) (Miura et al., 2018), Japanese rat snake (Iwanishi et al., 2018)		
	Birds	Chicken (Chang et al., 2006, 2007; Tobita-Teramoto et al., 2000)		
	Ungulates	Water buffalo (Damé et al., 2012), Cattle (Schmutz et al., 2004), Red deer (Reiner et al., 2020), Asinara donkey (Utzeri et al., 2016)		
	Rodents	House mouse (Yokoyama et al., 1990), Wistar rat (Blaszczyk et al., 2005), Domestic guinea pig (Yu et al., 2018)		
	Primates	Crab-eating macaque (Kim et al., 2017), Capuchin monkey (Galante Rocha de Vasconcelos et al., 2017), Hamadryas baboon (Koga et al., 2020), Human (reviewed in Montoliu et al., 2014)		
	Other mammals	Humpback whale (Polanowski et al., 2012), Ferret (Blaszczyk et al., 2007), American mink (Anistoroaei et al., 2008), Domestic cat (Imes et al., 2006; Lyons et al., 2005a; Schmidt-Küntzel et al., 2005), Silver fox (Yan et al., 2019)		
OCA2	Fish	Mexican cavefish (Gross and Wilkens, 2013), Lake Malawi cichlid (Kratochwil et al., 2019)	Cl^- channel regulating melanosome pH	Moderate loss of melanin
	Snakes	Corn snake (Saenko et al., 2015)		
	Mammals	Domestic dog (Caduff et al., 2017), Bama miniature pig (Zhang et al., 2019), House mouse (Shoji et al., 2015), Human (reviewed in Montoliu et al., 2014)		
TYRP1	Fish	Zebrafish (Krauss et al., 2014)	Enzymes contributing to melanin synthesis	Mild loss of melanin
	Birds	Saker falcon (Cortimiglia et al., 2017)		
	Mammals	Chinese indigenous pig (Ren et al., 2011), Liangshan pig (Wu et al., 2016), Domestic cat (Lyons et al., 2005b; Schmidt-Küntzel et al., 2005), Soay sheep (Gratten et al., 2007), Valais Red sheep (Paris et al., 2019), American mink (Cirera et al., 2016), Human (reviewed in Montoliu et al., 2014)		
TYRP2	Mammals	House mouse (Budd and Jackson, 1995; Jackson et al., 1992)		
SLC7A11	Mammals	House mouse (Chintala et al., 2005)	Solute transporters	
SLC24A5	Fish	Zebrafish (Lamason et al., 2005)		
	Mammals	Domestic dog (Winkler et al., 2014), Horse (Mack et al., 2017), Human (reviewed in Montoliu et al., 2014)		
SLC45A2	Fish	Japanese rice fish (Fukamachi et al., 2001)		
	Birds	Japanese quail (Gunnarsson et al., 2007), Chicken (Gunnarsson et al., 2007)		
	Mammals	Horse (Mariat et al., 2003), House mouse (Newton et al., 2001), Bengal tiger (Xu et al., 2013), Western lowland gorilla (Prado-Martinez et al., 2013), Human (reviewed in Montoliu et al., 2014)		

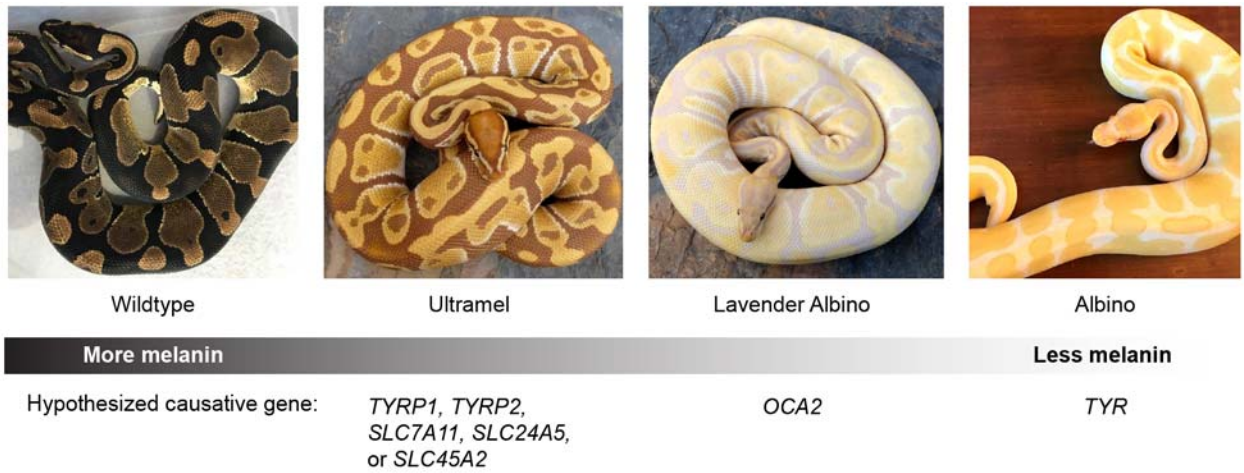

Figure 1. The Albino, Lavender Albino, and Ultramel color morphs have reduced brown-to-black coloration, characteristic of a loss of melanin. Red-to-yellow coloration is produced through non-melanin pigments and is unaffected in these morphs. Hypothesized causative genes represent genes in which loss-of-function variants in other vertebrates produce similar phenotypes (Table 1). Photo credits, Ryan Young of Molecular Reptile and Chiron Graves.

Results

Obtaining a reference sequence for melanogenesis genes in a wildtype ball python

Genes required for melanin production have been identified in humans and other vertebrates (Table 1). These genes encode enzymes that synthesize melanin (*TYR*, *TYRP1*, *TYRP2*) (Lai et al., 2018), a chloride channel required for maintaining the pH of melanosomes (*OCA2*) (Bellono et al., 2014), and transporters thought to import solutes into the cell or into organelles (*SLC7A11*, *SLC24A5*, and *SLC45A2*) (Chintala et al., 2005; Ginger et al., 2008; Vitavska and Wieczorek, 2013). These genes are highly conserved among vertebrates and occur in single copy in most vertebrate genomes. Loss-of-function variants in these genes in humans cause a genetic disorder known as oculocutaneous albinism, which is characterized by loss of melanin in the skin, hair, and eyes (Montoliu et al., 2014). This loss of melanin ranges from severe to mild, depending on the causative gene and exact genetics variants therein (Montoliu et al., 2014). Similar phenotypes occur in other animals, where the loss of melanin extends to feathers and scales (Table 1).

To obtain a reference sequence for melanogenesis genes in ball python, we amplified and sequenced the coding regions of *TYR*, *TYRP1*, *TYRP2*, *OCA2*, *SLC7A11*, *SLC24A5*, and *SLC45A2* from a single ball python having normal coloration (henceforth 'wildtype'). Primers for amplification were designed against the genome of Burmese python (*Python bivittatus*), the closest relative of ball python for which genome sequence was available (Castoe et al., 2013). Comparison of ball python sequences to sequences from Burmese python revealed 97.2-99.2% nucleotide identity within coding regions and 96.9-98.5% nucleotide identity within flanking non-coding regions (Table 2). This analysis provided a reference sequence for genes in ball python that might harbor loss-of-function variants causing the Albino, Lavender Albino, and Ultramel color morphs.

Table 2. Comparison of ball python and Burmese python genomic and protein sequences for melanogenesis genes.

Region	**Gene**	**Nucleotide identity (%)**	**Amino acid identity (%)**	**Total nucleotide sequence aligned (bp)**
Coding	*TYR*	98.5	99.6	1591
	TYRP1	99.2	99.6	1584
	TYRP2	98.3	99.1	1473
	OCA2	98.9	99.7	2577
	SLC7A11	98.7	99.7	1506
	SLC24A5	98.2	99.5	1379
	SLC45A2	97.2	98.9	1557
Non-coding	*TYR*	96.9	(not applicable)	577
	TYRP1	97.0		1160
	TYRP2	97.9		1060
	OCA2	98.5		2154
	SLC7A11	97.9		3407
	SLC24A5	97.9		1335
	SLC45A2	97.0		999

The Albino color morph is associated with three haplotypes of *TYR*

The Albino color morph in ball pythons is characterized by an absence or near absence of melanin in the skin and eyes. This phenotype resembles the phenotype caused by loss of function of *TYR* in other vertebrates. *TYR* encodes the enzyme catalyzing the rate-limiting step of melanin production (Lai et al., 2018). Loss of this enzymatic activity in other vertebrates causes a severe loss of melanin, which is typically more severe than the loss of melanin caused by loss of function of other melanogenesis genes (Table 1). We therefore hypothesized that the Albino color morph in ball pythons was caused by loss-of-function variants in *TYR*.

To test whether the Albino color morph was associated with variants in *TYR*, we performed a small-scale association study using 27 unrelated Albinos and 56 unrelated Non-Albinos, recruited from a total of 13 states in the United States. Polymorphic sites were identified through pilot sequencing of a subset of animals (see Methods), and each animal was genotyped at a total of six polymorphic sites in *TYR* (two near the 5' end of the gene and four near the 3' end) (Figure 2A). Haplotypes were reconstructed using PHASE, and association between color morph and haplotype was tested using the case-control test of PHASE (Stephens and Scheet, 2005; Stephens et al., 2001). As a negative control, we also tested for association between color morph and haplotype at *TYRP1*, *TYRP2*, and *OCA2*, using two polymorphic sites per gene (Table S1). This analysis revealed a significant association between color morph and haplotype at *TYR* ($p = 0.04$, Bonferroni corrected), but no association for the other three genes ($p > 0.05$, Bonferroni corrected). The association for TYR was driven by two features of the haplotype distribution: (i) diversity of *TYR* haplotypes among Albinos was reduced compared to Non-Albinos (three *TYR* haplotypes were found among Albinos, compared with 15 among Non-Albinos) and (ii) the two *TYR* haplotypes most common among Albinos were rare among Non-Albinos (these haplotypes have frequencies of 17-70% among Albinos, versus <1% among Non-Albinos) (Figure 2A). These results demonstrate and association between the Albino color

morph and variants in TYR, and they show that all Albino animals are homozygous or compound heterozygous for any of three haplotypes of *TYR*.

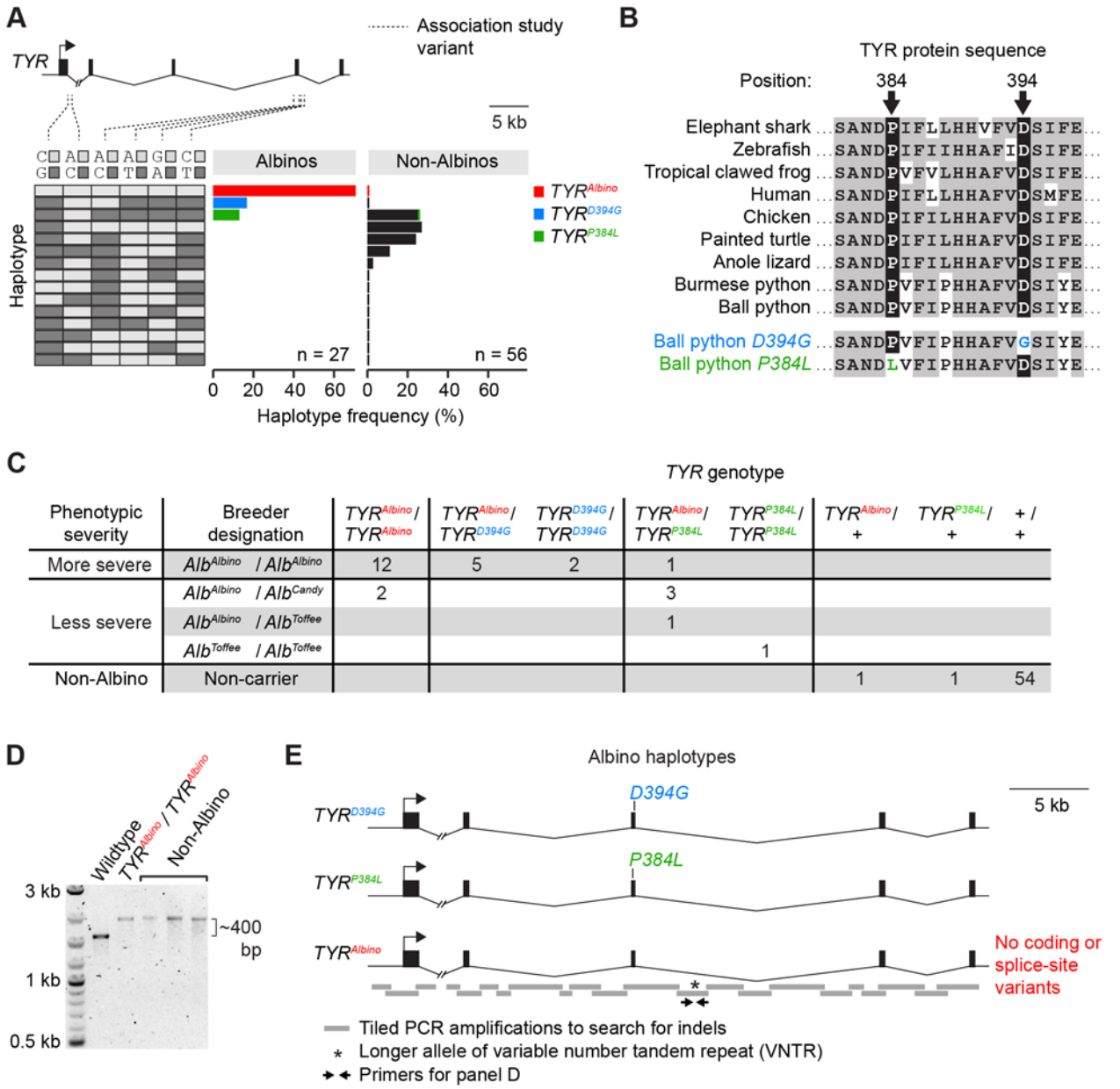

Phenotypic severity	Breeder designation	TYR Albino / TYR Albino	TYR Albino / TYR D394G	TYR D394G / TYR D394G	TYR Albino / TYR P384L	TYR P384L / TYR P384L	TYR Albino / +	TYR P384L / +	+ / +
More severe	Alb Albino / Alb Albino	12	5	2	1				
Less severe	Alb Albino / Alb Candy	2			3				
	Alb Albino / Alb Toffee				1				
	Alb Toffee / Alb Toffee					1			
Non-Albino	Non-carrier						1	1	54

Figure 2. The Albino color morph is associated with three haplotypes of *TYR*. (A) TYR haplotype frequencies among Albinos and Non-Albinos. (B) Alignment of *TYR* protein sequences surrounding the missense variants *D394G* and *P384L*. (C) *TYR* genotypes and breeder designations of animals used in the association study. +, any *TYR* haplotype found exclusively among Non-Albinos. (D) PCR amplification of a genomic fragment containing the variable number tandem repeat (VNTR) shown in E. Non-Albinos are examples of Non-Albinos homozygous for the longer allele of the VNTR. (E) Schematic of the three *TYR* haplotypes found in Albinos. The TYR^{Albino} haplotype contains no coding variants and no splice-site variants compared to wildtype. (A, E) Hash mark, discontinuity in the Burmese python reference genome.

We hypothesized that each of the three *TYR* haplotypes found among Albinos might carry a distinct loss-of-function variant in the gene. To search for such variants, we selected one Albino animal homozygous for each haplotype and sequenced the *TYR* coding regions and adjacent splice sites in these animals. We found that one of these animala was homozygous for an aspartic acid-to-glycine variant (*D394G*) in the third coding region of *TYR*. A second animal was homozygous for a proline-to-leucine variant (*P384L*), also in the third coding region of *TYR*. Both variants alter conserved residues (Figure 2B), and the *P384L* variant occurs at the same site as a similar variant (*P384A*) associated with oculocutaneous albinism in humans (Simeonov et al., 2013). The third animal carried no coding variants and no splice-site variants compared to wildtype. These results show that two of the three *TYR* haplotypes found among Albinos carried missense variants that are likely disruptive for TYR protein function. We term the *TYR* haplotypes carrying the missense variants TYR^{D394G} and TYR^{P384L}. We term the third Albino haplotype, which lacked coding or splice-site variants compared to wildtype, TYR^{Albino}.

We hypothesized that *D394G*, *P384L*, and an unidentified variant on the TYR^{Albino} haplotype were causative for the Albino color morph. This hypothesis predicts that animals homozygous or compound heterozygous for these variants will be Albino. Heterozygotes and non-carriers are predicted to be Non-Albino. To test this prediction, we genotyped our full panel of 27 Albinos and 56 Non-Albinos for the missense variants *D394G* and *P384L*. Consistent with our prediction, we found that animals homozygous or compound heterozygous for *D394G*, *P384L*, or the TYR^{Albino} haplotype were exclusively Albino (Figure 2C). Heterozygotes and non-carriers were exclusively Non-Albino (Figure 2C). The most common haplotype among Albinos was TYR^{Albino} (haplotype frequency of 70%), followed by TYR^{D394G} (17%) and TYR^{P384L} (13%). We conclude that *D394G*, *P384L*, and an unidentified variant on the TYR^{Albino} haplotype are likely causative for the Albino color morph; any combination of these variants produces the Albino phenotype.

Absence of an obvious loss-of-function variant on the *TYR*^{Albino} haplotype

The lack of coding or splice-site variants on *TYR*^{Albino} haplotype led us to hypothesize that this haplotype carried a loss-of-function variant in a non-coding region. To search for such variants, we examined the *TYR* promoter. We sequenced ~2 kb immediately upstream of the *TYR* start codon in a *TYR*^{Albino} homozygote and compared this sequence to wildtype. We found that the *TYR*^{Albino} haplotype differed from wildtype at a total three sites (three single-base substitutions). In all three cases, the *TYR*^{Albino} haplotype was homozygous for the allele shared with Burmese python (i.e. the ancestral allele). This result suggests that these variants are not causative for the Albino color morph. We conclude that the causative variant in the *TYR*^{Albino} haplotype does not reside within the sequenced region, ~2 kb upstream of the *TYR* start codon.

We hypothesized that the *TYR*^{Albino} haplotype might contain a large insertion or deletion (indel) in an intron that disrupts gene function. Intronic indels can disrupt slicing and have been found to disrupt the function of melanogenesis genes in other species (e.g. Cirera et al., 2016; Saenko et al., 2015). To search for large intronic indels in the *TYR*^{Albino} haplotype, we tiled PCR amplicons across *TYR* introns and compared amplicon sizes between a *TYR*^{Albino} homozygote and a wildtype animal. These amplicons tiled across a total of ~38 kb of intronic sequence, which included part of intron 1 and all of introns 2, 3, and 4 (Figure 2E). (Tiling across intron 1 was incomplete because this intron contains a discontinuity in the Burmese python reference genome. Amplification across this discontinuity was unsuccessful in ball python, even in wildtype.) Size differences between the TYR^{Albino} homozygote and wildtype were assessed via standard agarose gel electrophoresis, which we estimate was sensitive enough to reveal indels larger than ~50-100 bp, depending on amplicon size (which ranged from ~0.7-3.5 kb). This analysis revealed one size difference between the *TYR*^{Albino} homozygote and wildtype (Figure 2D). Sequencing of this amplicon showed that this size difference was caused by a variable number tandem repeat (VNTR) that was ~400 bp larger in the *TYR*^{Albino} homozygote than in

wildtype. Genotyping of the 56 Non-Albinos for this indel revealed that eight of these animals were homozygous for the larger allele of the VNTR (Figure 2D). This finding suggests that the larger allele of the VNTR is not causative for the Albino color morph. We propose that the *TYR*^{Albino} haplotype harbors a loss-of-function variant other than a large intronic indel or outside the genomic regions analyzed here.

TYR haplotypes do not perfectly correspond to Albino alleles recognized by breeders, but may predict phenotype severity

Ball python breeders describe the Albino color morph as having three alleles: *Alb*^{Albino}, *Alb*^{Candy}, and *Alb*^{Toffee}. Evidence for this view comes in part from variability in the coloration of Albino animals. The brown-to-black coloration observed in wildtype is entirely absent in some Albinos, and skin patches appear white. These Albinos are typically considered by breeders to be *Alb*^{Albino} homozygotes. Other Albinos show a less severe phenotype, where skin patches are faintly lavender instead of white. These Albinos are typically considered to carry one or more copies of *Alb*^{Candy} or *Alb*^{Toffee}.

We hypothesized that the Albino alleles recognized by breeders might correspond to the TYR haplotypes identified through sequencing (*TYR*^{D394G}, *TYR*^{P384L}, and *TYR*^{Albino}). To test this hypothesis, we examined the breeder designations of the 27 Albinos in our panel. Our panel included 20 animals designated as *Alb*^{Albino} homozygotes and seven animals designated as carrying one or more copies of *Alb*^{Candy} or *Alb*^{Toffee}. We found that breeder designations did not perfectly match *TYR* genotypes—animals with the same breeder designation sometimes had different *TYR* genotypes and vice versa (Figure 2C). Nonetheless, we found that animals designated by breeders as having one or more copies of *Alb*^{Candy} or *Alb*^{Toffee} were enriched for the *TYR*^{P384L} haplotype; animals designated as *Alb*^{Albino} homozygotes were enriched for the other two *TYR* haplotypes (*TYR*^{D394G} and *TYR*^{Albino}) ($p = 0.0014$, post-hoc Fisher's exact test). This association was imperfect and exceptions exist (Figure 2C). This pattern indicates that the

TYR^{P384L} haplotype is associated with less severe phenotypes, whereas the other two *TYR* haplotypes (*TYR*^{D394G} and *TYR*^{Albino}) are associated with more severe phenotypes. We conclude that *TYR* haplotypes do not perfectly correspond to the Albino color morph alleles recognized by breeders, but different *TYR* haplotypes may produce subtle differences in phenotypic severity.

The Lavender Albino color morph is associated with a deletion in *OCA2*

The Lavender Albino color morph is characterized by skin patches that are lavender instead of brown or black. This phenotype is thought to arise from melanin levels that are dramatically reduced but not entirely eliminated. Similar phenotypes have been observed in other vertebrates upon loss of function of *OCA2* (Table 1). *OCA2* encodes a chloride channel required for maintaining the pH of melanosomes (Bellono et al., 2014; Gardner et al., 1992). When the OCA2 protein is absent or non-functional, the enzymes that synthesize melanin are less active, and only small amounts of melanin are produced (Ni-Komatsu and Orlow, 2006; Puri et al., 2000). The resulting phenotype is typically less severe than the loss-of-function phenotype of *TYR*, but more severe than the loss-of-function phenotypes of other melanogenesis genes (Table 1). We therefore hypothesized that the Lavender Albino color morph was caused by loss-of-function variants in *OCA2*.

To search for loss-of-function variants in *OCA2*, we selected a single Lavender Albino animal and sequenced 23 of the 24 coding regions of *OCA2* in this animal. Comparison of these sequences to wildtype revealed no coding variants and no splice-site variants. We attempted to repeat this analysis for the remaining coding region (coding region 18), but we were unable to amplify this coding region from the Lavender Albino animal. Further test amplifications revealed that the Lavender Albino animal was homozygous for a 1,514-bp deletion spanning coding region 18 (Figure 3A-B). This deletion removes 36 amino acids from the protein and likely introduces a frameshift into the transcript, because the coding regions downstream of the deletion are out of frame compared to the coding regions upstream of the deletion (Figure 3E).

This frameshifted transcript is predicted to produce a protein that lacks six of the 12 transmembrane helices present in wildtype OCA2. Truncations occurring at similar positions in the OCA2 protein have been identified in humans and are associated with oculocutaneous albinism (Lee et al., 1994). We conclude that the deletion of *OCA2* coding region 18 likely disrupts protein function and is a strong candidate for the cause of the Lavender Albino color morph.

The Lavender Albino color morph is considered by breeders to have a single allele. We therefore predicted that the *OCA2* deletion would be shared by other Lavender Albino animals. We predicted that Non-Lavender Albinos would be heterozygous or non-carriers. To test this prediction, we genotyped the *OCA2* deletion in four unrelated Lavender Albinos, 76 unrelated Non-Lavender Albinos, and one unrelated animal described as heterozygous for the Lavender Albino color morph. We found that all four Lavender Albinos were homozygous for the deletion (Figure 3C-D). All 76 Non-Lavender Albinos were non-carriers. The animal reported to be heterozygous for Lavender Albino was heterozygous for the deletion. These findings support the conclusion that the *OCA2* deletion is causative for the Lavender Albino color morph (Figure 3E).

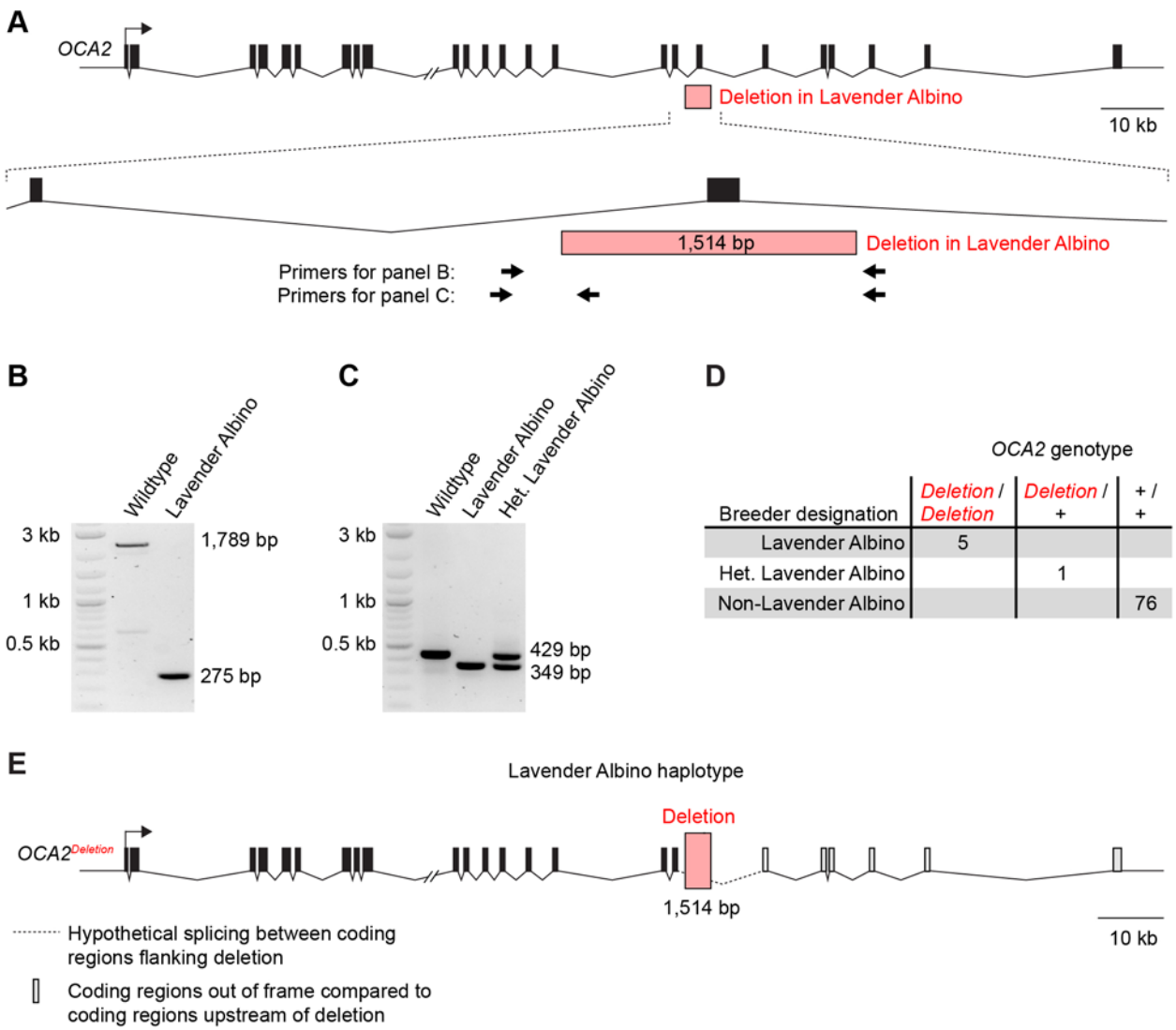

Figure 3. The Lavender Albino color morph is associated with a deletion in *OCA2*. (A) Schematic of the *OCA2* gene. (B) PCR amplification demonstrating the deletion in Lavender Albino. (C) PCR amplification used for genotyping the deletion in the animals in panel D. (D) Genotypes of five Lavender Albinos, 76 Non-Lavender Albinos, and one animal described as heterozygous for Lavender Albino. (E) Schematic of the *OCA2* haplotype found in Lavender Albinos. (A, E) Hash mark, discontinuity in the Burmese python reference genome.

The Ultramel color morph is associated with a missense variant and a putative deletion in *TYRP1*

The Ultramel color morph is characterized by skin patches that are tan or light brown, rather than dark brown or black. This phenotype suggests a mild loss of melanin and is similar to phenotypes in other vertebrates observed upon loss of function of any five genes: *TYRP1*,

TYRP2, *SLC7A11*, *SLC24A5*, and *SLC45A2* (Table 1). *TYRP1* and *TYRP2* encode enzymes involved in synthesizing melanin (Lai et al., 2018). Their enzymatic activities are partially reductant with other enzymes in the melanin synthesis pathway, and thus their loss-of-function phenotypes are milder compared to *TYR*. *SLC7A11* encodes a transporter responsible for importing cystine into the cell (Sato et al., 1999). Cystine is a precursor to some forms of melanin, and hence absence of the transporter alters melanin levels (Chintala et al., 2005). *SLC24A5* encodes a K^+-dependent Na^+-Ca^{2+} exchanger (Ginger et al., 2008), and *SLC45A2* encodes a putative sugar transporter (Vitavska and Wieczorek, 2013). Loss of either of these proteins causes a reduction in melanin, through mechanisms that may involve defects in regulation of melanosome pH (Bin et al., 2015; Ginger et al., 2008; Newton et al., 2001). The loss-of-function phenotypes of these genes in other vertebrates resembles the Ultramel color morph (Table 1), leading us to hypothesize that the Ultramel color morph was caused by loss-of-function variants in one of these genes.

To search for loss-of-function variants in *TYRP1*, *TYRP2*, *SLC7A11*, *SLC24A5*, and *SLC45A2*, we selected a single Ultramel animal and sequenced the coding regions of each of these genes in this animal. Comparison of these sequences to wildtype revealed a single coding variant: an arginine-to-histidine substitution (*R305H*) in coding region 4 of *TYRP1*. The Ultramel animal was homozygous for this variant. The arginine residue at this site is conserved across vertebrates (Figure 4A) and is also conserved in *TYR*, which is paralogous to *TYRP1* (Sturm et al., 1995). An arginine-to-histidine substitution at the homologous site in *TYR* has been reported in humans and is associated with oculocutaneous albinism (Gershoni-Baruch et al., 1994; Tripathi et al., 1992; Tsai et al., 1999), suggesting that a histidine at this site is disruptive to protein function. The *R305H* variant is therefore a good candidate for the cause of the Ultramel color morph.

The Ultramel color morph is considered by breeders to have a single allele. We therefore predicted that the *R305H* variant would be shared by other Ultramels. We predicted that Non-

Ultramels would be heterozygous or non-carriers. To test this prediction, we genotyped the *R305H* variant in two unrelated Ultramels and 78 unrelated Non-Ultramels. We found that one of the two Ultramels was homozygous for the *R305H* variant (Figure 4B). Neither the second Ultramel nor any of the 78 Non-Ultramels carried the *R305H* variant. This pattern is consistent with the *R305H* variant causing the Ultramel phenotype in Ultramels but not others.

We predicted that the Ultramel animal lacking the *R305H* variant carried an alternate loss-of-function allele of *TYRP1*. To test this prediction, we amplified and sequenced coding regions 1 through 5 of *TYRP1* in this animal. We found no coding variants and no splice-site variants compared to wildtype. We attempted to repeat this analysis for coding regions 6 and 7 of *TYRP1*, but we were unable to amplify these coding regions from the Ultramel lacking the *R305H* variant. Further test amplifications in the region indicated that these coding regions were missing from the genome this animal (Figure 4C). Loss of coding regions 6 and 7 was specific to Ultramel lacking the *R305H* variant and did not occur in the two Ultramels homozygous for the *R305H* variant, nor in any of the 78 Non-Ultramels (Figure 4B). A simple explanation of this pattern is that the Ultramel lacking the *R305H* variant was homozygous for a deletion spanning coding regions 6 and 7 of *TYRP1*. This putative deletion removes at least 2,208 bp from the genome and 117 amino acids from the TYRP1 protein, including the second of two zinc-binding domains. (The exact size and breakpoints of the putative deletion remain undetermined because the deletion extends into a discontinuity in the Burmese python reference genome.) Truncations occurring at similar positions in the TYRP1 protein have been identified in humans and are associated with oculocutaneous albinism (Forshew et al., 2005). We conclude that the Ultramel color morph is likely caused by variants in *TYRP1* and has two alleles: missense variant *R305H* and a putative deletion of coding regions 6 and 7 (Figure 4D).

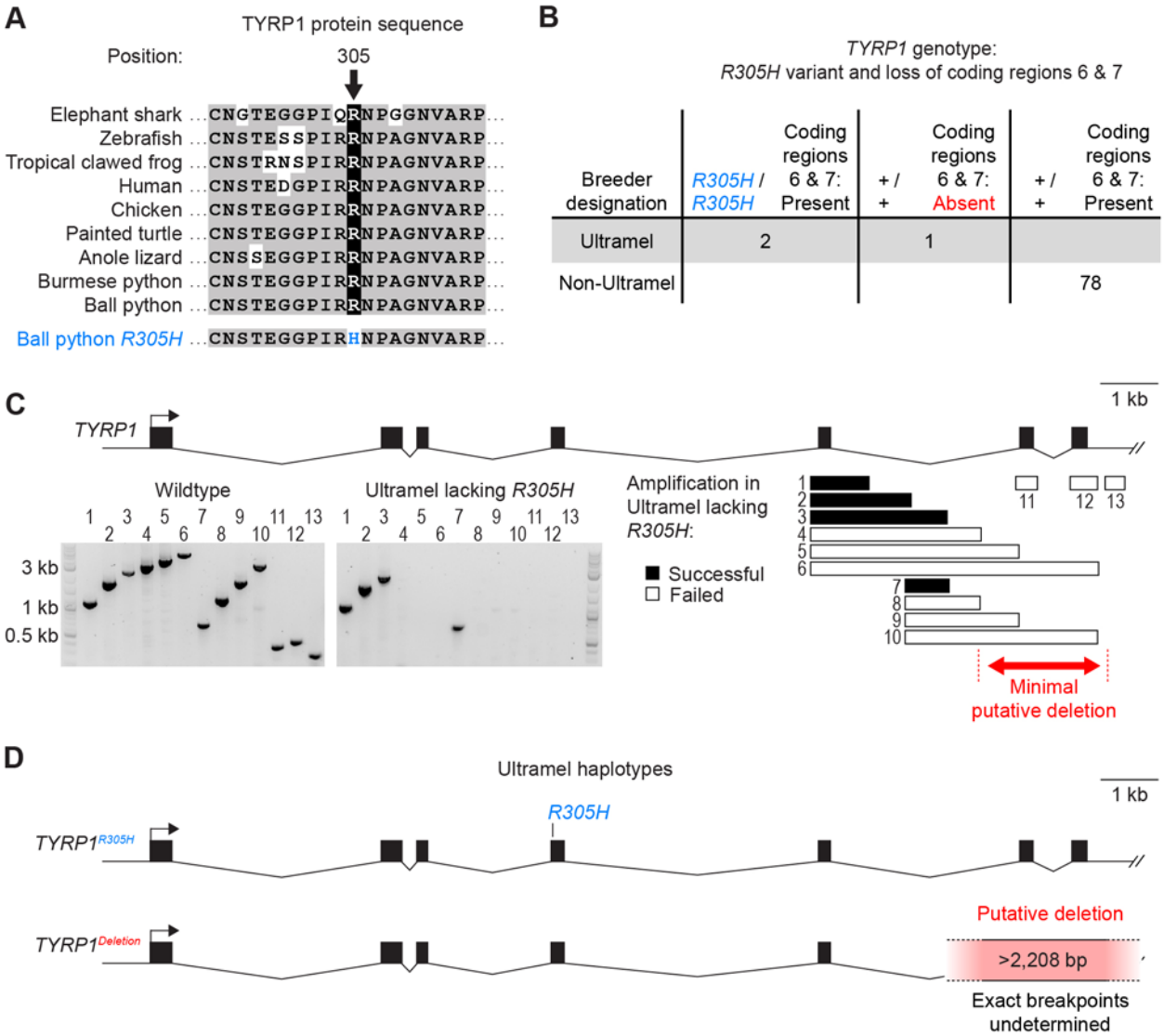

Figure 4. The Ultramel color morph is associated with a missense variant and a putative deletion in *TYRP1*. (A) Alignment of *TYRP1* protein sequence surrounding missense variant *R305H*. (B) Genotypes of three Ultramels and 78 Non-Ultramels. (C) Top, schematic of the *TYRP1* gene. Bottom left, PCR amplifications demonstrating the putative deletion in the Ultramel lacking *R305H*. Bottom right, alignment of PCR amplicons to the *TYRP1* gene. (D) Schematic of the two *TYRP1* haplotypes found in Ultramels. (A, D) Hash mark, discontinuity in the Burmese python reference genome.

Discussion

The goal of our study was to use pet samples recruited from the community to identify the genetic causes of the Albino, Lavender Albino, and Ultramel color morphs. We succeeded in recruiting three or more unrelated animals for each morph, along with larger number of

unrelated animals not belonging to these morphs. This sample size, albeit small, was sufficient to identify putatively causal variants for each morph (Figure 5). The Albino color morph was associated with three alleles of TYR: missense variant *D394G*, missense variant *P384L*, and haplotype TYR^{Albino}, which lacks coding or splice-site variants compared to wildtype. The Lavender Albino color morph was associated with a single allele of *OCA2*, a 1,514-bp deletion that removes *OCA2* coding region 18. The Ultramel color morph was associated with two alleles of *TYRP1*: missense variant *R305H* and a putative deletion that removes *TYRP1* coding regions 6 and 7. These findings are consistent with genetic data from other vertebrates (Table 1), indicating that the loss-of-function phenotypes of *TYR*, *OCA2*, and *TYRP1* range from severe (*TYR*) to moderate (*OCA2*) to mild (*TYPR1*). Our study demonstrates that pet ball pythons are a tractable resource for genetic analysis of coloration in reptiles, at least for color morphs having obvious candidate genes.

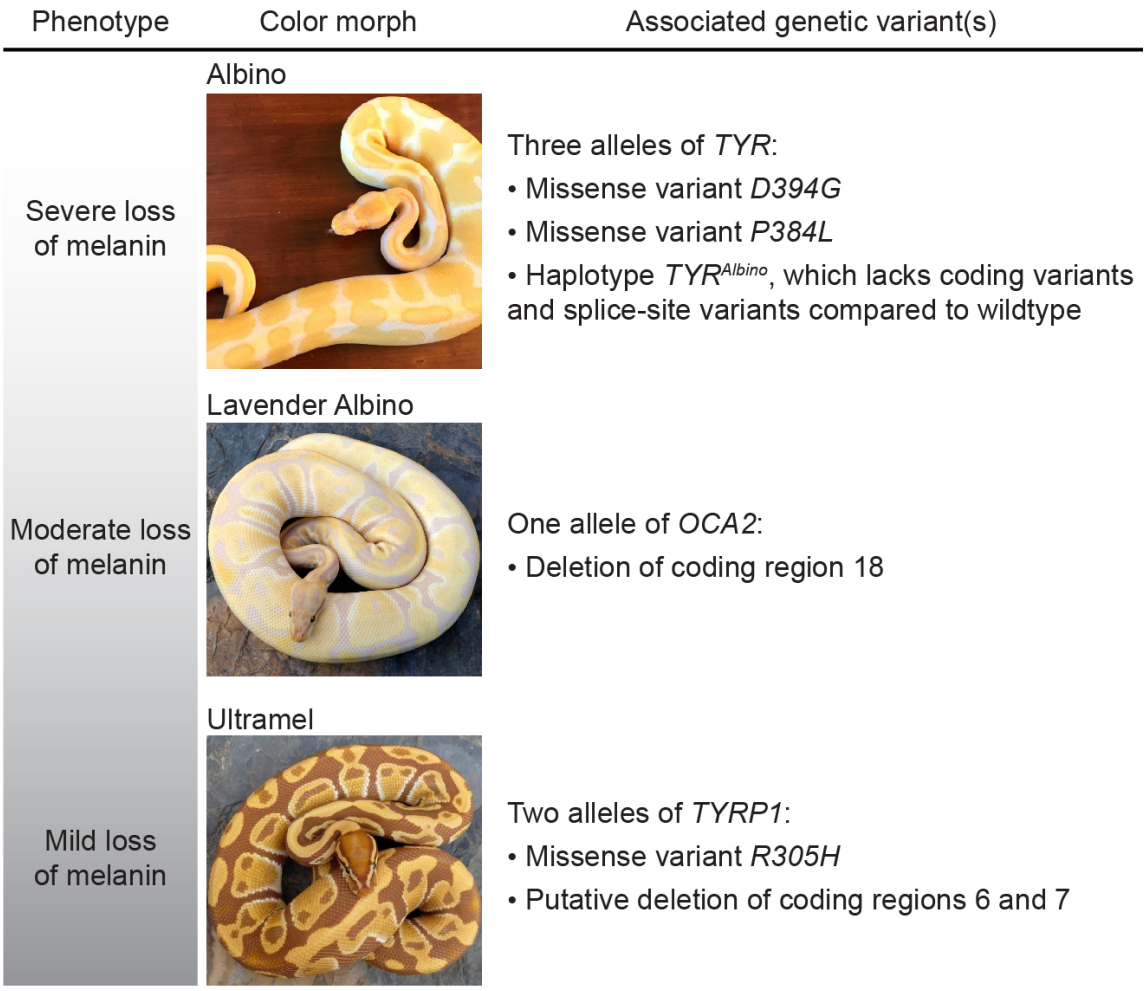

Figure 5. Summary of genetic variants associated with the Albino, Lavender Albino, and Ultramel color morphs. Photo credits, Ryan Young of Molecular Reptile and Chiron Graves.

Molecular functions of genetic variants associated with color morphs

The missense variants and deletions found in *TYR*, *TYRP1*, and *OCA2* are likely hypomorphic or null alleles. The deletion in *OCA2* likely results in a frameshifted transcript that, if not degraded by nonsense-mediated decay, encodes a protein lacking six of the 12 transmembrane helices present in wildtype OCA2 (Gardner et al., 1992). This truncated protein is therefore unlikely to retain the Cl^- channel activity observed for wildtype OCA2 (Bellono et al., 2014). *TYR* and *TYPR1* encode globular enzymes that require copper or zinc as co-factors (Lai et al., 2018). Variants *P384L* and *D394G* in *TYR* reside in the second of TYR's two copper-binding domains and may therefore alter the ability of the TYR to bind copper. Variant *R305H* in

TYRP1 occurs at a site that normally forms salt bridges with residues located elsewhere in the peptide chain (Lai et al., 2018). An arginine-to-histidine substitution at this site likely disrupts these salt bridges and may therefore interfere with proper protein folding. The putative deletion in *TYRP1* removes the C-terminal ~20% of the protein. This deleted region includes the second of TYRP1's two zinc-binding domains and several alpha helices residing to the enzyme's hydrophobic core (Lai et al., 2018). Truncated TYRP1 protein is therefore unlikely to fold properly, nor can it properly associate with zinc.

The TYR^{Albino} haplotype is the most common *TYR* haplotype found among Albinos, but it lacks an obvious loss-of-function variant. This haplotype contains no coding variants, no splice-site variants, no derived variants within 2 kb upstream of the start codon, and no large indels in three of four introns (with the exception of a longer allele of a VNTR, which is not specific to the TYR^{Albino} haplotype). We propose that the TYR^{Albino} haplotype contains a loss-of-function variant not detectable by methods used in the current study. Examples include regulatory variants farther upstream of the start codon, substitutions in introns that disrupt slicing, or large indels or rearrangements involving the first intron. Cryptic loss-of-function variants in melanogenesis genes are thought to be relatively common in humans, where ~10-20% of oculocutaneous albinism patients are heterozygous for pathogenic variants in a known melanogenesis gene but lack a coding or splice-site variant on the opposite allele (Lasseaux et al., 2018; Rooryck et al., 2008, 2009).

Multiple alleles of the Albino color morph

Prior to the current study, the Albino color morph was recognized by breeders as having three alleles: Alb^{Albino}, Alb^{Candy}, and Alb^{Toffee}. This idea arose from the Albino color morph being discovered independently at least three times and from slight phenotypic variability among Albino animals. Some animals have skin patches that are white (a more severe phenotype), whereas others have skin patches that are faintly lavender (a less severe phenotype). Prior to

the current study, it remained unclear whether the Albino alleles recognized by breeders represented distinct molecular variants in the causative gene.

Our results confirm that the Albino color morph has three molecular alleles: TYR^{D394G}, TYR^{P384L}, and TYR^{Albino}. These alleles do not perfectly correspond to the alleles recognized by breeders, although the TYR^{P384L} haplotype is enriched among animals with less severe phenotypes (i.e. animals described as carrying Alb^{Candy} or Alb^{Toffee}). We speculate that the TYR^{P384L} haplotype was discovered twice and was named Alb^{Candy} by one breeder and Alb^{Toffee} by another breeder. We speculate that TYR^{D394G} and TYR^{Albino} were not previously recognized by breeders as distinct. These haplotypes roughly correspond to what breeders recognized as Alb^{Albino}. The less severe phenotype associated with TYR^{P384L} may reflect the *P384L* variant being less disruptive to gene function compared with variants on the other two haplotypes. Alternatively, the less severe phenotype associated with TYR^{P384L} may reflect genetic linkage to modifiers in other genes.

Our study demonstrates that the Albino allele designations current in use by breeders are not an accurate reflection of molecular genotype. Renaming of the Albino alleles is warranted, although we recognize that owners and breeders may be resistant to renaming due to cultural attachment to existing allele names.

Multiple alleles of the Ultramel color morph

Our finding of multiple *TYRP1* alleles for the Ultramel color morph was unexpected. This morph was not previously described as having multiple alleles. We speculate that one of two alleles associated with the Ultramel color morph may represent an allele originally associated with a morph known as Caramel Albino. Caramel Albinos have coloration similar to Ultramels, but have been disfavored among owners and breeders because Caramel Albino females are sometimes infertile. Caramel Albinos were not included in our study because we were unable to recruit Caramel Albino samples. We speculate that the Caramel Albino morph is allelic with

Ultramel, and that one of two *TYRP1* alleles associated with Ultramel may represent the allele originally described as Caramel Albino. This allele may have been rebranded by some breeders as Ultramel to avoid the stigma associated with infertility. Future genotyping of Caramel Albinos is needed to test whether Caramel Albino is associated with variants in *TYRP1*.

Prospects for genetic testing

Many breeders of ball pythons wish to identify heterozygotes of recessive color morphs. Currently the only tool for identifying heterozygotes is test breeding, which is slow and laborious. The results of the current study will enable simple genetic testing for Albino, Lavender Albino, and Ultramel. A major advantage of genetic testing is that tests can be performed prior to reproductive maturity, as early as the first shed. Testing for Lavender Albino can be performed by genotyping the *OCA2* deletion. Testing for Albino can be performed by sequencing the *TYR* missense variants *D395G* and *P384L*, and by genotyping variants that distinguish the TYR^{Albino} haplotype from other *TYR* haplotypes. Detection of *D395G* or *P384L* should be considered diagnostic for Albino because these variants are likely causative for the Albino color morph. Detection of the TYR^{Albino} haplotype is less diagnostic because the causative variant on TYR^{Albino} haplotype remains unknown. Testing for one of the two Ultramel alleles can be performed by sequencing the *TYRP1* missense variant *R305H*. The other Ultramel allele—the putative deletion of *TYRP1* coding regions 6 and 7—cannot currently be detected in heterozygotes using simple methods because the breakpoints of this putative deletion are unknown. We expect that these genetic tests will facilitate breeding of Albino, Lavender Albino, and Ultramel animals.

Ball pythons as a genetic system

The market for pet ball pythons is huge, and many owners prefer animals with novel color patterns. This demand has led breeders to propagate genetic variants affecting coloration (Broghammer, 2019; McCurley, 2005). This effort has fortuitously created a collection of "mutants" useful for understanding the genetics of coloration in reptiles. Examples include ball

python morphs with altered red-to-yellow coloration (e.g. Axanthic) and morphs in which the normal mottled color pattern is converted to dorsal strips (e.g. Clown, Genetic Stripe, Super Stripe). Red-to-yellow pigments are largely uncharacterized in reptiles (although see McLean et al., 2017; Ullate-Agote et al., 2020), and morphs affecting these pigments may provide insight into the metabolism and storage of these pigments. Morphs with stripes are reminiscent of evolutionary changes in color patterning across snake species (Allen et al., 2013) and may provide insights into the developmental mechanisms by which these changes evolve. Future studies of ball python color morphs will be aided by our groundwork showing that ball python samples can be recruited effectively from pet owners, and that genetic analyses in ball python can be scaffolded using the genome of Burmese python as a reference. Similar groundwork has also been provided by a recent study characterizing the ball python morph known as Piebald (Garcia-Elfring et al., 2020). We expect that a continued community-science approach will be effective in developing ball pythons into a resource for understanding the genetics of reptile coloration.

Methods

Recruitment of ball python sheds

Ball python sheds were recruited from pet owners and breeders by placing announcements in Twitter, Reddit, and Facebook, and by contacting sellers having active listings on Morph Market (www.morphmarket.com). Contributors were instructed to allow sheds to dry (if wet) and to ship sheds via standard first-class mail. Contributors sending multiple sheds were instructed to package sheds individually in plastic bags during shipping. Contributors were not provided monetary compensation for sheds, although some contributors were given pre-paid shipping envelopes to cover shipping costs. Contributors were thanked via social media whenever possible. Upon receipt, sheds were stored at -20°C to kill any insect larvae infesting the sheds.

Animals were considered unrelated if their sheds were contributed by different contributors, or if their sheds were contributed by the same contributor, but the contributor indicated that the animals had been obtained from different breeders. The total set of animals were 27 Albinos, five Lavender Albinos, three Ultramels, one animal described as heterozygous for Lavender Albino, and 46 animals described as having normal coloration (i.e. wildtype) or belonging to color morphs other than Albino, Lavender Albino, or Ultramel. None of these animals were described as heterozygous for Albino or Ultramel. All animals were included in all parts of the study, except for the Lavender Albino heterozygote, which was only included in the Lavender Albino study.

Performing experiments in an undergraduate laboratory course

The majority of experiments and analyses described in this study were performed by undergraduate students as part of a laboratory course at Eastern Michigan University (BIO306). This practice required that our experimental design rely on simple techniques, namely PCR and Sanger sequencing. To avoid student errors in these techniques, we implemented the following

precautions. First, students never extracted DNA from more than one animal within the same laboratory period. Second, students performed negative and positive control reactions for all PCR amplifications. Data from students having incorrect controls were excluded from analysis. Third, all sequence analyses were performed independently by three or more students. When the results of all students did not all agree, sequences were re-analyzed by the instructor (HSS).

Annotation of melanogenesis genes in Burmese python

Our analyses in ball python used the genome of Burmese python as a reference. We therefore required high-confidence gene annotations in Burmese python for the genes used in our study (*TYR*, *TYRP1*, *TYRP2*, *OCA2*, *SLC7A11*, *SLC24A5*, and *SLC45A2*). Preliminary inspection of existing gene annotations in Burmese python suggested that many gene annotations contained errors. A main cause of these errors was that the Burmese python genome (*Python_molurus_bivittatus-5.0.2*) is a scaffold-level assembly; many genes were split across scaffolds. We therefore curated new gene annotations in Burmese python, using conservation of gene structure across species. We aligned protein sequences for each gene from corn snake, anole lizard, chicken, and/or mouse, and compared these alignments to genomic sequences from each species. This analysis revealed that the positions of coding-region boundaries relative to protein sequences were largely conserved for all seven genes (Table S2). We therefore concluded that the positions of these boundaries were likely conserved in Burmese python and could be used to curate new gene annotations.

To curate new gene annotations, we performed TBLASTN searches of the Burmese python genome (*Python_molurus_bivittatus-5.0.2*) using protein sequences from anole lizard or corn snake as the query. Hits were examined manually, and gene annotations were built to match the coding-region boundaries conserved across species. Details for each gene annotation are given below.

***TYR*:** The Burmese python genome was queried using TYR protein sequence from anole lizard (XP_003219419.1). The N-terminus of this query (coding region 1) hit Burmese python transcript XM_007438960.1 on scaffold 4418. The C-terminus of this query (coding regions 2 to 5) hit Burmese python transcript XM_007436041.2 on scaffold 3103. TYR was annotated as the union of these transcripts. The 3' boundary of coding region 1 was adjusted to match the boundary conserved across species (…TTC TCT TCA TGG CAA-3').

***TYRP1*:** The Burmese python genome was queried using TYRP1 protein sequence from corn snake (XP_034266320.1). The N-terminus of this query (coding regions 1 to 5) hit Burmese python transcript XM_007426971.3 on scaffold 801. The C-terminus of this query (coding regions 6 and 7) hit unannotated regions on this same scaffold. *TYRP1* was annotated as the union of transcript XM_007426971.3 and coding regions 6 and 7. The boundaries of coding regions 6 and 7 were built to match the boundaries conserved across species (coding region 6, 5'-ATA TCT CAA CAT ACC....AAG TTC AGT GGC CAT-3'; coding region 7, 5'-CAC AAG CTC TCC ATG....CAG TCA GAT GTG TGA-3').

***TYRP2*:** The Burmese python genome was queried using TYRP2 protein sequence from corn snake (XP_034273310.1). The N-terminus of this query (coding regions 1 to 3) hit unannotated regions on Burmese python scaffold 4970. The C-terminus of this query (coding regions 4 to 8) hit Burmese python transcript XM_025174219.1 on this same scaffold. *TYRP2* was annotated as the union of coding regions 1 to 3 and C-terminal five coding regions of transcript XM_025174219.1. Transcript XM_025174219.1 contains a sixth coding region that does not match *TYRP2* and was therefore excluded from the gene annotation. The boundaries of coding regions 1 to 3 were built to match the boundaries conserved across species (coding region 1, 5'-ATG GCC TTC CTG CTG....GTT GCC AAT GCA CAG-3'; coding region 2, 5'-GAC ATT TTG CTG GCT....GAG ATA CTC TAT TAG-3'; coding region 3, 5'- GAC CAG GCC GTC CCT....GAA AGA GAT CTG CAG-3').

***OCA2*:** The Burmese python genome was queried using OCA2 protein sequence from corn snake (XP_034287267.1). The N-terminus of this query (coding regions 1 to 9) hit Burmese python transcript XM_025173964.1 on scaffold 4704. The C-terminus of this query (coding regions 10 to 24) hit Burmese python transcript XM_007433276.1 on scaffold 2194. *OCA2* was annotated as the union of these transcripts. The 5' boundary of coding region 10 was adjusted to match the boundary conserved across species (5'-ATT GTC CAC AGG ACA…).

***SLC7A11*:** The Burmese python genome was queried using SLC7A11 protein sequence from corn snake (XP_034257397.1). All regions of the query hit Burmese python transcript XM_007430906.3 on scaffold 1543. *SLC7A11* was annotated as transcript XM_007430906.3, with no further adjustments.

***SLC24A5*:** The Burmese python genome was queried using SLC24A5 protein sequence from corn snake (XP_034290605.1) extended at its N-terminus to an upstream start codon present in the parent transcript (XM_034434714.1). The N-terminus of the query (coding region 1) hit an unannotated region on Burmese python scaffold 3984. The C-terminus of this query (coding regions 2 to 9) hit Burmese python transcript XM_007438007.2 on this same scaffold. *SLC24A5* was annotated as the union of coding region 1 and transcript XM_007438007.2. The boundaries of coding region 1 were built to match the boundaries conserved across species (5'-ATG CAG CCT GCC GAG....TCC GCG AGG ATC CCG -3'). The 5' boundary of coding region 2 was adjusted to match the boundary conserved across species (5'-AGA ACG AAA CCC GCT...).

***SLC45A2*:** The Burmese python genome was queried using *SLC45A2* protein sequence from corn snake (XP_034298386.1). The N-terminal region of this query (coding regions 1 and 2) hit Burmese python transcript XM_007432459.2 on scaffold 1939. The C-terminal region of this query (coding regions 5 to 7) hit Burmese python transcript XM_007437721.2 on scaffold 3858. *SLC45A2* was annotated as the union of these transcripts.

DNA extraction

Sheds were rinsed in tap water to remove dirt and debris. Sheds were air dried and lysed overnight at ~60˚C in ~1 ml lysis buffer (100 mM Tris-HCl pH 8.0, 100 mM EDTA, 2% sodium dodecyl sulfate, 3 mM $CaCl_2$, 2 mg/ml Proteinase K) per ~8 cm^2 piece of shed. Lysate was separated from visible fragments of undigested shed and further cleared by centrifugation at 13,000 x g for 2 min. To precipitate protein, ammonium acetate was added to supernatant to a final concentration of 1.875 M. Samples were incubated on ice for 10 min and centrifuged at 13,000 x g for 3-5 min at 4˚C. Supernatant was mixed with an equal volume of magnetic bead mixture (10 mM Tris-HCl pH 8.0, 1 mM EDTA, 1.6 M NaCl, 0.2% Tween-20, 11% polyethylene glycol, 0.04% washed SpeedBeads [Sigma #GE45152105050250]), and samples shaken for 10 min. Beads were separated from supernatant using a magnet, washed twice in 0.2 ml 70% ethanol for 2 min, and air dried for ~1 min. DNA was eluted from beads in TE buffer (10 mM Tris-HCl pH 8.0, 1 mM EDTA) at 65°C for >5 min.

Primer design and PCR

Primers were designed against the genome of Burmese python or against genomic sequences from ball python obtained in an earlier step of the study. Primers were designed using Primer3 (Untergasser et al., 2012), using default parameters and a target annealing temperature of 60°C. Amplification was first tested at 57°C, to allow for occasional divergence between ball python and Burmese python genomic sequences. In some cases, annealing temperatures were later adjusted to 52°C, 60°C, or 61°C, to obtain stronger product or to eliminate background bands.

Genomic fragments were amplified using OneTaq polymerase (NEB #M0480) or Q5 polymerase (NEB #M0491). Genotyping assays described below used OneTaq, unless otherwise specified. OneTaq reactions consisted of 1X OneTaq Standard Reaction Buffer, 200 µM dNTPs, 0.2 µM of each primer, and 0.025 U/µl OneTaq polymerase. OneTaq thermocycling

conditions were as follows: 94°C for 2 min; 30-35 cycles of 94°C for 30 sec, 52-61°C for 30 sec, and 68°C for 1-4 min; and 68°C for 5 min. Q5 reactions consisted of 1X Q5 Reaction Buffer, 200 µM dNTPs, 0.5 µM of each primer, and 0.02 U/µl Q5 polymerase. Q5 thermocycling conditions were as follows: 98°C for 30 sec; 30-35 cycles of 98°C for 10 sec, 58-61°C for 15 sec, and 72°C for 1.5-3 min; and 72°C for 5 min. Reactions used 10-100 ng template DNA per 20 µl volume.

Sanger sequencing

PCR products were purified for Sanger sequencing using magnetic beads or gel extraction. For magnetic-bead purification, PCR reactions were mixed with three volumes of magnetic-bead mixture (10 mM Tris-HCl pH 8.0, 1 mM EDTA, 1.6-2.5 M NaCl, 0.2% Tween-20, 11-20% polyethylene glycol, 00.04% washed SpeedBeads [Sigma #GE45152105050250]), and agitated for 5 min. Beads were separated from supernatant using a magnet, washed twice in 0.2 ml 80% ethanol for >30 sec, and air-dried for 30 sec. PCR products were eluted from beads in 10 mM Tris-HCl pH 8.0 for >3 min at 65°C. Gel extraction was performed using QIAquick Gel Extraction Kit (Qiagen #28704), according to the manufacturer guidelines. Sanger sequencing was performed by Eton Bioscience Inc (etonbio.com).

Sequencing of coding regions and comparison to Burmese python

Coding regions of melanogenesis genes were amplified and sequenced using primers given in Table S3. Chromatograms were trimmed using SnapGene Viewer (snapgene.com/snapgene-viewer) and aligned to one another or to genomic sequences from Burmese python using ApE (jorgensen.biology.utah.edu/wayned/ape). Alignments were examined manually to identify divergent and polymorphic sites. Sequence identity between ball python and Burmese python was calculated across alignable sequence, excluding indels.

Association study genotyping

Variants for the association study were identified through amplification and pilot sequencing of genomic fragments from five animals (thee Non-Albinos, one Albino, and one Ultramel). For *TYR*, *TYRP1*, and *TYRP2*, we identified one or more genomic fragments containing multiple polymorphic sites within the same amplicon. These genomic fragments were selected for the association study. For *OCA2*, we did not identify any genomic fragments containing multiple polymorphic sites; we therefore selected two genomic fragments each containing a single polymorphic site. Divergence between the Albino animal and the other four animals was not a criterion for inclusion of variants in the association study. Variants were genotyped by amplifying and sequencing genomic fragments containing the variants. Locations of variants and primers used to amplify and sequence variants are given in Table S1.

Haplotype reconstruction

Haplotypes were reconstructed using PHASE version 2.1 (Stephens and Scheet, 2005; Stephens et al., 2001), using 200 iterations, a thinning interval of 2, and a burn-in parameter of 100. This combination of parameters produced identical or nearly identical output for seven runs seeded with different random numbers (therefore meeting the criteria for effective parameter settings, according to the PHASE documentation). The case-control permutation test was performed by compared Albinos to Non-Albinos.

Genotyping assays for *TYR*

TYR missense variants *D394G* and *P384L* were genotyped by amplifying and sequencing a genomic fragment containing *TYR* coding region 3. This fragment was amplified using primers 13F (5'-ACT TTC AGG TGG GCA GCA G-3') and 13R (5'-GCT GAC AAC TAA AAT CTC TGC AA-3') and an annealing temperature of 52°C. The amplicon was sequenced using primer 13F.

TYR promoter and intronic regions are amplified using primers given in Table S4. Promoter fragments were sequenced in full, and intronic fragments were sequenced from one end, to confirm that the correct region of the genome had been amplified. Sequencing primers are given in Table S4. Size differences among intronic fragments were assessed by separating fragments on a 1.25% agarose gel. Gels were run long enough for the shortest ladder band (100 bp) to migrate ~8 cm from its starting position.

Allele sizes of the variable number tandem repeat (VNTR) in *TYR* were genotyped by amplifying a genomic fragment located in *TYR* intron 3, using primers 214F (5'-TCT CAC CTG ATG GCA CAT TC-3') and 209R (5'-GTG CCC ACC CTG ATG TTA TT-3') and an annealing temperature of 60°C. Amplicon sizes were analyzed as for intronic fragments, described above.

Genotyping assays for *OCA2*

The *OCA2* deletion was initially identified by amplifying and sequencing a genomic fragment spanning *OCA2* coding region 18. This fragment was amplified using primers 218F (5'-ACC CCG TAG CCT CTT CAA AT-3') and 166R (5'-TGG GTG GCA AAC AAT CAT AA-3'), an annealing temperature of 60°C, and Q5 polymerase. Amplicons were sequenced using both primers.

The *OCA2* deletion was genotyped after its initial identification using a three-primer PCR assay. This assayed used one forward primer and two reverse primers. The forward primer and one of the reverse primers were located outside the deletion: 217F (5'-GGA GAG AGA ATC CAA CCC TTG -3') and 166R (5'-TGG GTG GCA AAC AAT CAT AA-3'). The second reverse primer was located within the deletion: 188R (5'-CAA AGA CCA TTG TCC ATT TCC-3'). The annealing temperature was 57°C. This assay produces a 429-bp product for the wildtype allele and a 349-bp product for the deletion allele. Heterozygotes produce both products.

Genotyping assays for *TYRP1*

TYRP1 missense variant *R305H* was genotyped by amplifying and sequencing a genomic fragment spanning *TYRP1* coding region 4. This fragment was amplified using primers 18F (5'-GCT CTT TTC TCT AAG TCT GAC CTC -3') and 18R (5'-TCT TGT CCC ACA AAA GGA TTT -3') and an annealing temperature of 57°C. The amplicon was sequenced using primer 18F.

The putative deletion of *TYRP1* coding regions 6 and 7 was identified using primers given in Table S5. The putative deletion was genotyped after its initial identification by amplifying a genomic fragment of *TYRP1* spanning coding regions 6 and 7. This fragment was amplified using primers 20F (5'-GCA TTG TTT TAT CAG CCA TGA A-3') and 21R (5'-GGA ATT GAG ACA AAT CCT TGG-3') and an annealing temperature of 57°C.

Protein sequence alignment

Protein sequences were aligned using Clustal Omega (Sievers et al., 2011), using default parameters.

Data availability

Genotypes are provided in Table S6. DNA sequences have been submitted to GenBank. GenBank accession numbers have not yet been assigned, but will be added here once they become available.

Acknowledgements

We thank Matt Rockman and Katy Greenwald for advice on haplotype reconstruction; Bob Winning, Anne Casper, and David Kass for comments on the manuscript; and the Educational Course Support program of New England BioLabs for reagents used in undergraduate teaching labs. We thank the following individuals for contributing ball python sheds: Adam and Nicole Schmid; Alycia Butler; Andelyn Czajka; Brad Carter of Driftless Reptiles; Chiron Graves; Chun Ku of Dynasty Reptiles; Daniel Ross; David Wolf of Tornado Alley Reptiles; Dawn and Kelsi Greene of Super Natural Balls; Dayna Plehn; Debby Brauer; Eric Chung of Chung Reptiles; Erin Burt; Haily McCullough; Jamie Palazzo of New Day Reptiles; Jodi Wilkowski; John Cordone of Blue Water Reptiles; Jordan Noland; Justin Kobylka of J. Kobylka Reptiles; Lindsay VanOrman; Lisa Huis; Mark Bilger; Maryann Barbon; Mia Hynes; Michael, Lisa, and Bodie Cole of Ballroom Pythons South; Morgan Evans and Michael Kitto of MK Pythons; Morgan Shelton; Paul and Amber Fiorito of Vivid Scales; Pets 'n' Things of Saline, MI; Rachel Voyt; Ryan Young of Molecular Reptile; Stephanie S. Crisp; Steve P. of Prime Pets; and several anonymous contributors. We thank the following individuals for providing images of color morphs: Beth Woodyard; Cat Church; Cormier Jason; Christine Miller; Darin Taylor; Daniel Hatcher; David C. Callahan; Donald Grinstead; Elijah Snyder; Innovative Ectotherms; Jake Lewis; Jessica Allison; Jessica Van Riper; Justin Kobylka; James Thompson; Justin Revington; Mariette van Vuuren; Mark Hopkins; Mark Smith; Matthew Lopez; Morgan Evans; Robert Cooper; Ron Heisenberg; and Ryan Young.

Student in the BIO306 Consortium were Alexandra Ernst, Alia Frederick, Alissa Zoltowski, Amber Northcutt, Andraya Ackerman, Anna Pathammavong, Annette Miller, Ashly Matzek, Asra Akhlaq, Aubrey Martin, Bailey Knight, Benjamin Huff, Beth Wasserman, Brian Donald Condron, Caleb Sommer, Cassandra Rigor, Charles Southwell, Chase Chitwood, Chelsea Brown, Christina Roka, Ciarra Womack, Clay McKenzie, Daniela Nappo, Darby

Fracassa, Deirdre McCarter, Dhruvalkumar Patel, Dominic Paoletti, Drake Dzierwa, Erica R. Geml, Erin Bissett, Ezekiel Butcher, Garrett Chance, Garry Lewis, Genesis Garmendia, Geo Joy, Hajer Musa Abuzir, Haley Praski, Hanan Alroaini, Iqra Akhlaq, Ismael Yasin, Janelle Aethyr, Janelle Janisse, Jayce Alee Perysian, Jemar Rooks, Jonathan Chang, Jonathan Harris, Joseph H. Oberlitner, Joshua Mason, Juwan Taylor, Kailynn Sparks, Karissa Urban, Karli Siefman, Kealy Szymanski, Kelsy Roque, Keyan Marshall, Khaled Ali, Karleigh Hassenzahl, Kylie Powrie, Lauren Colone, Lissette Rosas, Manoj Perumallapalli, Mariam Samir, Maryam Nimer, Maya Mackey, Megan McNulty, Mel Roberts, Micaela Schempf, Molly Cook, Myah Kelly, Nahiel Sukar, Natalie Diaz, Natasha MacKay, Nathan Barnett, Nathaniel Gonzalez, Noura Taybeh, Pablo De la Vega, Rida Ali, Ronnie Bryans, Ryan Elliott, Saja Hussein, Samantha Glowacki, Samuel Teener, Sarah Holtzen, Sarah Schmidt, Shanti Bernstein, Shelan Mizuree, Smarpita Singh, Stevie Zabrosky, Taia Broadbent, Tommiea Robertson, Tyler Schallhorn, Verginio Persicone, William Soder, Wolfgang Ebersole, and Yvette Campbell.

Funding information

This work was supported by a Faculty Research Fellowship and James H. Brickley Award from Eastern Michigan University to HSS and an Undergraduate Research Stimulus Program Award and a Don Brown and Meta Hellwig Undergraduate Research Award from Eastern Michigan University to ARB. The funders had no role in study design, data collection and analysis, decision to publish, or preparation of the manuscript.

Competing interests

The authors have declared that no competing interests exist.

References

Allen, W.L., Baddeley, R., Scott-Samuel, N.E., and Cuthill, I.C. (2013). The evolution and function of pattern diversity in snakes. Behavioral Ecology *24*, 1237–1250.

Anistoroaei, R., Fredholm, M., Christensen, K., and Leeb, T. (2008). Albinism in the American mink (Neovison vison) is associated with a tyrosinase nonsense mutation. Anim Genet *39*, 645–648.

Bagnara, J.T., and Matsumoto, J. (2008). Comparative Anatomy and Physiology of Pigment Cells in Nonmammalian Tissues. In The Pigmentary System: Physiology and Pathophysiology, 2nd Edition, (Wiley-Blackwell), p.

Bagnara, J.T., Taylor, J.D., and Hadley, M.E. (1968). The dermal chromatophore unit. J Cell Biol *38*, 67–79.

Bagnara, J.T., Fernandez, P.J., and Fujii, R. (2007). On the blue coloration of vertebrates. Pigment Cell Res *20*, 14–26.

Bale, R. (2020). Ball python exports raise concerns as demand for the popular pet grows. National Geographic.

Bellono, N.W., Escobar, I.E., Lefkovith, A.J., Marks, M.S., and Oancea, E. (2014). An intracellular anion channel critical for pigmentation. ELife *3*, e04543.

Bin, B.-H., Bhin, J., Yang, S.H., Shin, M., Nam, Y.-J., Choi, D.-H., Shin, D.W., Lee, A.-Y., Hwang, D., Cho, E.-G., et al. (2015). Membrane-Associated Transporter Protein (MATP) Regulates Melanosomal pH and Influences Tyrosinase Activity. PLoS One *10*, e0129273.

Blaszczyk, W.M., Arning, L., Hoffmann, K.-P., and Epplen, J.T. (2005). A Tyrosinase missense mutation causes albinism in the Wistar rat. Pigment Cell Res *18*, 144–145.

Blaszczyk, W.M., Distler, C., Dekomien, G., Arning, L., Hoffmann, K.-P., and Epplen, J.T. (2007). Identification of a tyrosinase (TYR) exon 4 deletion in albino ferrets (Mustela putorius furo). Anim Genet *38*, 421–423.

Broghammer, S. (2019). Python regius: Atlas of Colour Morphs Keeping and Breeding (NTV Natur und Tier-Verlag).

Budd, P.S., and Jackson, I.J. (1995). Structure of the mouse tyrosinase-related protein-2/dopachrome tautomerase (Tyrp2/Dct) gene and sequence of two novel slaty alleles. Genomics *29*, 35–43.

Burbrink, F.T., and Castoe, T.A. (2011). Molecular Phylogeography of Snakes. In Snakes: Ecology and Conservation, (Cornell University Press), p.

Caduff, M., Bauer, A., Jagannathan, V., and Leeb, T. (2017). OCA2 splice site variant in German Spitz dogs with oculocutaneous albinism. PLoS One *12*, e0185944.

Castoe, T.A., de Koning, A.P.J., Hall, K.T., Card, D.C., Schield, D.R., Fujita, M.K., Ruggiero, R.P., Degner, J.F., Daza, J.M., Gu, W., et al. (2013). The Burmese python genome reveals the molecular basis for extreme adaptation in snakes. Proc Natl Acad Sci U S A *110*, 20645–20650.

Chang, C.-M., Coville, J.-L., Coquerelle, G., Gourichon, D., Oulmouden, A., and Tixier-Boichard, M. (2006). Complete association between a retroviral insertion in the tyrosinase gene and the recessive white mutation in chickens. BMC Genomics *7*, 19.

Chang, C.M., Furet, J.P., Coville, J.L., Coquerelle, G., Gourichon, D., and Tixier-Boichard, M. (2007). Quantitative effects of an intronic retroviral insertion on the transcription of the tyrosinase gene in recessive white chickens. Anim Genet *38*, 162–167.

Chintala, S., Li, W., Lamoreux, M.L., Ito, S., Wakamatsu, K., Sviderskaya, E.V., Bennett, D.C., Park, Y.-M., Gahl, W.A., Huizing, M., et al. (2005). Slc7a11 gene controls production of pheomelanin pigment and proliferation of cultured cells. Proc Natl Acad Sci U S A *102*, 10964–10969.

Cieslak, M., Reissmann, M., Hofreiter, M., and Ludwig, A. (2011). Colours of domestication. Biological Reviews *86*, 885–899.

Cirera, S., Markakis, M.N., Kristiansen, T., Vissenberg, K., Fredholm, M., Christensen, K., and Anistoroaei, R. (2016). A large insertion in intron 2 of the TYRP1 gene associated with American Palomino phenotype in American mink. Mamm Genome *27*, 135–143.

Cooke, T.F., Fischer, C.R., Wu, P., Jiang, T.-X., Xie, K.T., Kuo, J., Doctorov, E., Zehnder, A., Khosla, C., Chuong, C.-M., et al. (2017). Genetic Mapping and Biochemical Basis of Yellow Feather Pigmentation in Budgerigars. Cell *171*, 427-439.e21.

Cortimiglia, C., Castiglioni, B., Pizzi, F., Stella, A., and Capra, E. (2017). Involvement of tyrosinase-related protein 1 gene in the light brown plumage phenotype of Falco cherrug. Anim Genet *48*, 125–126.

Cuthill, I.C., Allen, W.L., Arbuckle, K., Caspers, B., Chaplin, G., Hauber, M.E., Hill, G.E., Jablonski, N.G., Jiggins, C.D., Kelber, A., et al. (2017). The biology of color. Science *357*.

Damé, M.C.F., Xavier, G.M., Oliveira-Filho, J.P., Borges, A.S., Oliveira, H.N., Riet-Correa, F., and Schild, A.L. (2012). A nonsense mutation in the tyrosinase gene causes albinism in water buffalo. BMC Genet *13*, 62.

Forshew, T., Khaliq, S., Tee, L., Smith, U., Johnson, C.A., Mehdi, S.Q., and Maher, E.R. (2005). Identification of novel TYR and TYRP1 mutations in oculocutaneous albinism. Clin Genet *68*, 182–184.

Fukamachi, S., Shimada, A., and Shima, A. (2001). Mutations in the gene encoding B, a novel transporter protein, reduce melanin content in medaka. Nat Genet *28*, 381–385.

Galante Rocha de Vasconcelos, F.T., Hauzman, E., Dutra Henriques, L., Kilpp Goulart, P.R., de Faria Galvão, O., Sano, R.Y., da Silva Souza, G., Lynch Alfaro, J., de Lima Silveira, L.C., Fix Ventura, D., et al. (2017). A novel nonsense mutation in the tyrosinase gene is related to the albinism in a capuchin monkey (Sapajus apella). BMC Genet *18*, 39.

Garcia-Elfring, A., Roffey, H.L., Hendry, A.P., and Barrett, R.D.H. (2020). A nonsense mutation in TFEC is the likely cause of the recessive piebald phenotype in ball pythons (Python regius). BioRxiv 2020.10.30.362970.

Gardner, J.M., Nakatsu, Y., Gondo, Y., Lee, S., Lyon, M.F., King, R.A., and Brilliant, M.H. (1992). The Mouse Pink-Eyed Dilution Gene: Association with Human Prader-Willi and Angelman Syndromes. Science *257*, 1121–1124.

Gazda, M.A., Araújo, P.M., Lopes, R.J., Toomey, M.B., Andrade, P., Afonso, S., Marques, C., Nunes, L., Pereira, P., Trigo, S., et al. (2020). A genetic mechanism for sexual dichromatism in birds. Science *368*, 1270–1274.

Gershoni-Baruch, R., Rosenmann, A., Droetto, S., Holmes, S., Tripathi, R.K., and Spritz, R.A. (1994). Mutations of the tyrosinase gene in patients with oculocutaneous albinism from various ethnic groups in Israel. Am J Hum Genet *54*, 586–594.

Ghiradella, H. (1985). Structure and Development of Iridescent Lepidopteran Scales: the Papilionidae as a Showcase Family. Annals of the Entomological Society of America *78*, 252–264.

Ginger, R.S., Askew, S.E., Ogborne, R.M., Wilson, S., Ferdinando, D., Dadd, T., Smith, A.M., Kazi, S., Szerencsei, R.T., Winkfein, R.J., et al. (2008). SLC24A5 encodes a trans-Golgi network protein with potassium-dependent sodium-calcium exchange activity that regulates human epidermal melanogenesis. J Biol Chem *283*, 5486–5495.

Gratten, J., Beraldi, D., Lowder, B.V., McRae, A.F., Visscher, P.M., Pemberton, J.M., and Slate, J. (2007). Compelling evidence that a single nucleotide substitution in TYRP1 is responsible for coat-colour polymorphism in a free-living population of Soay sheep. Proc Biol Sci *274*, 619–626.

Gross, J.B., and Wilkens, H. (2013). Albinism in phylogenetically and geographically distinct populations of Astyanax cavefish arises through the same loss-of-function Oca2 allele. Heredity (Edinb) *111*, 122–130.

Gunnarsson, U., Hellström, A.R., Tixier-Boichard, M., Minvielle, F., Bed'hom, B., Ito, S., Jensen, P., Rattink, A., Vereijken, A., and Andersson, L. (2007). Mutations in SLC45A2 cause plumage color variation in chicken and Japanese quail. Genetics *175*, 867–877.

Guo, L., Bloom, J., Sykes, S., Huang, E., Kashif, Z., Pham, E., Ho, K., Alcaraz, A., Xiao, X.G., Duarte-Vogel, S., et al. (2021). Genetics of white color and iridophoroma in "Lemon Frost" leopard geckos. BioRxiv 2020.12.18.423549.

Huang, D., Lewis, V.M., Toomey, M.B., Corbo, J.C., and Parichy, D.M. (2021). Development and genetics of red coloration in the zebrafish relative Danio albolineatus. BioRxiv 2021.05.11.443569.

Imes, D.L., Geary, L.A., Grahn, R.A., and Lyons, L.A. (2006). Albinism in the domestic cat (Felis catus) is associated with a tyrosinase (TYR) mutation. Anim Genet *37*, 175–178.

Irizarry, K.J.L., and Bryden, R.L. (2016). In Silico Analysis of Gene Expression Network Components Underlying Pigmentation Phenotypes in the Python Identified Evolutionarily Conserved Clusters of Transcription Factor Binding Sites. Adv Bioinformatics *2016*, 1286510.

Iwanishi, S., Zaitsu, S., Shibata, H., and Nitasaka, E. (2018). An albino mutant of the Japanese rat snake (Elaphe climacophora) carries a nonsense mutation in the tyrosinase gene. Genes Genet Syst *93*, 163–167.

Jackson, I.J., Chambers, D.M., Tsukamoto, K., Copeland, N.G., Gilbert, D.J., Jenkins, N.A., and Hearing, V. (1992). A second tyrosinase-related protein, TRP-2, maps to and is mutated at the mouse slaty locus. EMBO J *11*, 527–535.

Kim, Y.-H., Park, S.-J., Choe, S.-H., Lee, J.-R., Cho, H.-M., Kim, S.-U., Kim, J.-S., Sim, B.-W., Song, B.-S., Lee, Y., et al. (2017). Identification and characterization of the tyrosinase gene (TYR) and its transcript variants (TYR_1 and TYR_2) in the crab-eating macaque (Macaca fascicularis). Gene *630*, 21–27.

Kimura, T., Nagao, Y., Hashimoto, H., Yamamoto-Shiraishi, Y., Yamamoto, S., Yabe, T., Takada, S., Kinoshita, M., Kuroiwa, A., and Naruse, K. (2014). Leucophores are similar to xanthophores in their specification and differentiation processes in medaka. PNAS *111*, 7343–7348.

Kinoshita, S., and Yoshioka, S. (2005). Structural colors in nature: the role of regularity and irregularity in the structure. Chemphyschem *6*, 1442–1459.

Koga, A., Wakamatsu, Y., Kurosawa, J., and Hori, H. (1999). Oculocutaneous albinism in the i6 mutant of the medaka fish is associated with a deletion in the tyrosinase gene. Pigment Cell Res *12*, 252–258.

Koga, A., Hisakawa, C., and Yoshizawa, M. (2020). Baboon bearing resemblance in pigmentation pattern to Siamese cat carries a missense mutation in the tyrosinase gene. Genome *63*, 275–279.

Kratochwil, C.F., Urban, S., and Meyer, A. (2019). Genome of the Malawi golden cichlid fish (Melanochromis auratus) reveals exon loss of oca2 in an amelanistic morph. Pigment Cell Melanoma Res *32*, 719–723.

Krauss, J., Geiger-Rudolph, S., Koch, I., Nüsslein-Volhard, C., and Irion, U. (2014). A dominant mutation in tyrp1A leads to melanophore death in zebrafish. Pigment Cell Melanoma Res *27*, 827–830.

Kwon, Y.M., Vranken, N., Hoge, C., Lichak, M.R., Francis, K.X., Camacho-Garcia, J., Bista, I., Wood, J., McCarthy, S., Chow, W., et al. (2021). Genomic consequences of domestication of the Siamese fighting fish. BioRxiv 2021.04.29.442030.

Lai, X., Wichers, H.J., Soler-Lopez, M., and Dijkstra, B.W. (2018). Structure and Function of Human Tyrosinase and Tyrosinase-Related Proteins. Chemistry *24*, 47–55.

Lamason, R.L., Mohideen, M.-A.P.K., Mest, J.R., Wong, A.C., Norton, H.L., Aros, M.C., Jurynec, M.J., Mao, X., Humphreville, V.R., Humbert, J.E., et al. (2005). SLC24A5, a putative cation exchanger, affects pigmentation in zebrafish and humans. Science *310*, 1782–1786.

Lasseaux, E., Plaisant, C., Michaud, V., Pennamen, P., Trimouille, A., Gaston, L., Monfermé, S., Lacombe, D., Rooryck, C., Morice-Picard, F., et al. (2018). Molecular characterization of a series of 990 index patients with albinism. Pigment Cell Melanoma Res *31*, 466–474.

Lee, S.T., Nicholls, R.D., Bundey, S., Laxova, R., Musarella, M., and Spritz, R.A. (1994). Mutations of the P gene in oculocutaneous albinism, ocular albinism, and Prader-Willi syndrome plus albinism. N Engl J Med *330*, 529–534.

Liu, Q., Qi, Y., Liang, Q., Song, J., Liu, J., Li, W., Shu, Y., Tao, M., Zhang, C., Qin, Q., et al. (2019). Targeted disruption of tyrosinase causes melanin reduction in Carassius auratus cuvieri and its hybrid progeny. Sci China Life Sci *62*, 1194–1202.

Lopes, R.J., Johnson, J.D., Toomey, M.B., Ferreira, M.S., Araujo, P.M., Melo-Ferreira, J., Andersson, L., Hill, G.E., Corbo, J.C., and Carneiro, M. (2016). Genetic Basis for Red Coloration in Birds. Curr Biol *26*, 1427–1434.

Lyons, L.A., Imes, D.L., Rah, H.C., and Grahn, R.A. (2005a). Tyrosinase mutations associated with Siamese and Burmese patterns in the domestic cat (Felis catus). Anim Genet *36*, 119–126.

Lyons, L.A., Foe, I.T., Rah, H.C., and Grahn, R.A. (2005b). Chocolate coated cats: TYRP1 mutations for brown color in domestic cats. Mamm Genome *16*, 356–366.

Mack, M., Kowalski, E., Grahn, R., Bras, D., Penedo, M.C.T., and Bellone, R. (2017). Two Variants in SLC24A5 Are Associated with “Tiger-Eye” Iris Pigmentation in Puerto Rican Paso Fino Horses. G3 (Bethesda) *7*, 2799–2806.

Mariat, D., Taourit, S., and Guérin, G. (2003). A mutation in the MATP gene causes the cream coat colour in the horse. Genet Sel Evol *35*, 119–133.

McCurley, K. (2005). Complete Ball Python, A Comprehensive Guide to Care, Breeding, and Genetic Mutations (ECO / Serpent’s Tale NHBD).

McLean, C.A., Lutz, A., Rankin, K.J., Stuart-Fox, D., and Moussalli, A. (2017). Revealing the Biochemical and Genetic Basis of Color Variation in a Polymorphic Lizard. Mol Biol Evol *34*, 1924–1935.

Meredith, P., and Sarna, T. (2006). The physical and chemical properties of eumelanin. Pigm. Cell. Res. *19*, 572–594.

Miura, I., Tagami, M., Fujitani, T., and Ogata, M. (2018). Spontaneous tyrosinase mutations identified in albinos of three wild frog species. Genes Genet Syst *92*, 189–196.

Montoliu, L., Grønskov, K., Wei, A.-H., Martínez-García, M., Fernández, A., Arveiler, B., Morice-Picard, F., Riazuddin, S., Suzuki, T., Ahmed, Z.M., et al. (2014). Increasing the complexity: new genes and new types of albinism. Pigment Cell Melanoma Res *27*, 11–18.

Mundy, N.I., Stapley, J., Bennison, C., Tucker, R., Twyman, H., Kim, K.-W., Burke, T., Birkhead, T.R., Andersson, S., and Slate, J. (2016). Red Carotenoid Coloration in the Zebra Finch Is Controlled by a Cytochrome P450 Gene Cluster. Curr Biol *26*, 1435–1440.

Newton, J.M., Cohen-Barak, O., Hagiwara, N., Gardner, J.M., Davisson, M.T., King, R.A., and Brilliant, M.H. (2001). Mutations in the human orthologue of the mouse underwhite gene (uw) underlie a new form of oculocutaneous albinism, OCA4. Am J Hum Genet *69*, 981–988.

Ni-Komatsu, L., and Orlow, S.J. (2006). Heterologous expression of tyrosinase recapitulates the misprocessing and mistrafficking in oculocutaneous albinism type 2: Effects of altering intracellular pH and pink-eyed dilution gene expression. Experimental Eye Research *82*, 519–528.

Nüsslein-Volhard, C., and Singh, A.P. (2017). How fish color their skin: A paradigm for development and evolution of adult patterns: Multipotency, plasticity, and cell competition regulate proliferation and spreading of pigment cells in Zebrafish coloration. Bioessays *39*.

Olsson, M., Stuart-Fox, D., and Ballen, C. (2013). Genetics and evolution of colour patterns in reptiles. Semin Cell Dev Biol *24*, 529–541.

Paris, J.M., Letko, A., Häfliger, I.M., Ammann, P., Flury, C., and Drögemüller, C. (2019). Identification of two TYRP1 loss-of-function alleles in Valais Red sheep. Anim Genet *50*, 778–782.

Polanowski, A.M., Robinson-Laverick, S.M., Paton, D., and Jarman, S.N. (2012). Variation in the tyrosinase gene associated with a white humpback whale (Megaptera novaeangliae). J Hered *103*, 130–133.

Prado-Martinez, J., Hernando-Herraez, I., Lorente-Galdos, B., Dabad, M., Ramirez, O., Baeza-Delgado, C., Morcillo-Suarez, C., Alkan, C., Hormozdiari, F., Raineri, E., et al. (2013). The genome sequencing of an albino Western lowland gorilla reveals inbreeding in the wild. BMC Genomics *14*, 363.

Prum, R. (2006). The anatomy, physics and evolution of avian structural color. In Bird Coloration, (Harvard University Press), p.

Puri, N., Gardner, J.M., and Brilliant, M.H. (2000). Aberrant pH of Melanosomes in Pink-Eyed Dilution (p) Mutant Melanocytes. J Invest Dermatol *115*, 607–613.

Reiner, G., Tramberend, K., Nietfeld, F., Volmer, K., Wurmser, C., Fries, R., and Willems, H. (2020). A genome-wide scan study identifies a single nucleotide substitution in the tyrosinase gene associated with white coat colour in a red deer (Cervus elaphus) population. BMC Genet *21*, 14.

Ren, J., Mao, H., Zhang, Z., Xiao, S., Ding, N., and Huang, L. (2011). A 6-bp deletion in the TYRP1 gene causes the brown colouration phenotype in Chinese indigenous pigs. Heredity (Edinb) *106*, 862–868.

Rooryck, C., Morice-Picard, F., Elçioglu, N.H., Lacombe, D., Taieb, A., and Arveiler, B. (2008). Molecular diagnosis of oculocutaneous albinism: new mutations in the OCA1-4 genes and practical aspects. Pigment Cell Melanoma Res *21*, 583–587.

Rooryck, C., Morice, F., Lacombe, D., Taieb, A., and Arveiler, B. (2009). Genetic basis of oculocutaneous albinism. Expert Review of Dermatology *4*, 611–622.

Saenko, S.V., Teyssier, J., van der Marel, D., and Milinkovitch, M.C. (2013). Precise colocalization of interacting structural and pigmentary elements generates extensive color pattern variation in Phelsuma lizards. BMC Biol *11*, 105.

Saenko, S.V., Lamichhaney, S., Martinez Barrio, A., Rafati, N., Andersson, L., and Milinkovitch, M.C. (2015). Amelanism in the corn snake is associated with the insertion of an LTR-retrotransposon in the OCA2 gene. Sci Rep *5*, 17118.

Sato, H., Tamba, M., Ishii, T., and Bannai, S. (1999). Cloning and expression of a plasma membrane cystine/glutamate exchange transporter composed of two distinct proteins. J Biol Chem *274*, 11455–11458.

Schmidt-Küntzel, A., Eizirik, E., O'Brien, S.J., and Menotti-Raymond, M. (2005). Tyrosinase and tyrosinase related protein 1 alleles specify domestic cat coat color phenotypes of the albino and brown loci. J Hered *96*, 289–301.

Schmutz, S.M., Berryere, T.G., Ciobanu, D.C., Mileham, A.J., Schmidtz, B.H., and Fredholm, M. (2004). A form of albinism in cattle is caused by a tyrosinase frameshift mutation. Mamm Genome *15*, 62–67.

Shawkey, M.D., and D'Alba, L. (2017). Interactions between colour-producing mechanisms and their effects on the integumentary colour palette. Philos Trans R Soc Lond B Biol Sci *372*.

Shoji, H., Kiniwa, Y., Okuyama, R., Yang, M., Higuchi, K., and Mori, M. (2015). A nonsense nucleotide substitution in the oculocutaneous albinism II gene underlies the original pink-eyed dilution allele (Oca2(p)) in mice. Exp Anim *64*, 171–179.

Sievers, F., Wilm, A., Dineen, D., Gibson, T.J., Karplus, K., Li, W., Lopez, R., McWilliam, H., Remmert, M., Söding, J., et al. (2011). Fast, scalable generation of high-quality protein multiple sequence alignments using Clustal Omega. Mol Syst Biol *7*, 539.

Simeonov, D.R., Wang, X., Wang, C., Sergeev, Y., Dolinska, M., Bower, M., Fischer, R., Winer, D., Dubrovsky, G., Balog, J.Z., et al. (2013). DNA variations in oculocutaneous albinism: an updated mutation list and current outstanding issues in molecular diagnostics. Hum Mutat *34*, 827–835.

Singh, A.P., and Nüsslein-Volhard, C. (2015). Zebrafish stripes as a model for vertebrate colour pattern formation. Curr Biol *25*, R81–R92.

Slominski, A., Tobin, D.J., Shibahara, S., and Wortsman, J. (2004). Melanin pigmentation in mammalian skin and its hormonal regulation. Physiol. Rev. *84*, 1155–1228.

Stephens, M., and Scheet, P. (2005). Accounting for decay of linkage disequilibrium in haplotype inference and missing-data imputation. Am J Hum Genet *76*, 449–462.

Stephens, M., Smith, N.J., and Donnelly, P. (2001). A new statistical method for haplotype reconstruction from population data. Am J Hum Genet *68*, 978–989.

Sturm, R.A., O'Sullivan, B.J., Box, N.F., Smith, A.G., Smit, S.E., Puttick, E.R., Parsons, P.G., and Dunn, I.S. (1995). Chromosomal structure of the human TYRP1 and TYRP2 loci and comparison of the tyrosinase-related protein gene family. Genomics *29*, 24–34.

Tobita-Teramoto, T., Jang, G.Y., Kino, K., Salter, D.W., Brumbaugh, J., and Akiyama, T. (2000). Autosomal albino chicken mutation (ca/ca) deletes hexanucleotide (-deltaGACTGG817) at a copper-binding site of the tyrosinase gene. Poult Sci *79*, 46–50.

Toews, D.P.L., Hofmeister, N.R., and Taylor, S.A. (2017). The Evolution and Genetics of Carotenoid Processing in Animals. Trends Genet. *33*, 171–182.

Toomey, M.B., Lopes, R.J., Araújo, P.M., Johnson, J.D., Gazda, M.A., Afonso, S., Mota, P.G., Koch, R.E., Hill, G.E., Corbo, J.C., et al. (2017). High-density lipoprotein receptor SCARB1 is required for carotenoid coloration in birds. Proc Natl Acad Sci U S A *114*, 5219–5224.

Tripathi, R.K., Strunk, K.M., Giebel, L.B., Weleber, R.G., and Spritz, R.A. (1992). Tyrosinase gene mutations in type I (tyrosinase-deficient) oculocutaneous albinism define two clusters of missense substitutions. Am J Med Genet *43*, 865–871.

Tsai, C.H., Tsai, F.J., Wu, J.Y., Lin, S.P., Chang, J.G., Yang, C.F., and Lee, C.C. (1999). Insertion/deletion mutations of type I oculocutaneous albinism in chinese patients from Taiwan. Hum Mutat *14*, 542.

Ullate-Agote, A., Burgelin, I., Debry, A., Langrez, C., Montange, F., Peraldi, R., Daraspe, J., Kaessmann, H., Milinkovitch, M.C., and Tzika, A.C. (2020). Genome mapping of a LYST mutation in corn snakes indicates that vertebrate chromatophore vesicles are lysosome-related organelles. PNAS *117*, 26307–26317.

Untergasser, A., Cutcutache, I., Koressaar, T., Ye, J., Faircloth, B.C., Remm, M., and Rozen, S.G. (2012). Primer3--new capabilities and interfaces. Nucleic Acids Res *40*, e115.

Utzeri, V.J., Bertolini, F., Ribani, A., Schiavo, G., Dall'Olio, S., and Fontanesi, L. (2016). The albinism of the feral Asinara white donkeys (Equus asinus) is determined by a missense mutation in a highly conserved position of the tyrosinase (TYR) gene deduced protein. Anim Genet *47*, 120–124.

Vitavska, O., and Wieczorek, H. (2013). The SLC45 gene family of putative sugar transporters. Mol Aspects Med *34*, 655–660.

Winkler, P.A., Gornik, K.R., Ramsey, D.T., Dubielzig, R.R., Venta, P.J., Petersen-Jones, S.M., and Bartoe, J.T. (2014). A partial gene deletion of SLC45A2 causes oculocutaneous albinism in Doberman pinscher dogs. PLoS One *9*, e92127.

Wu, X., Zhang, Y., Shen, L., Du, J., Luo, J., Liu, C., Pu, Q., Yang, R., Li, X., Bai, L., et al. (2016). A 6-bp deletion in exon 8 and two mutations in introns of TYRP1 are associated with blond coat color in Liangshan pigs. Gene *578*, 132–136.

Xu, X., Dong, G.-X., Hu, X.-S., Miao, L., Zhang, X.-L., Zhang, D.-L., Yang, H.-D., Zhang, T.-Y., Zou, Z.-T., Zhang, T.-T., et al. (2013). The genetic basis of white tigers. Curr Biol *23*, 1031–1035.

Yan, S., Zhao, D., Hu, M., Tan, X., Lai, W., Kang, J., Yu, F., Li, Y., and Bai, C. (2019). A single base insertion in the tyrosinase gene is associated with albino phenotype in silver foxes (Vulpes vulpes). Anim Genet *50*, 550.

Yokoyama, T., Silversides, D.W., Waymire, K.G., Kwon, B.S., Takeuchi, T., and Overbeek, P.A. (1990). Conserved cysteine to serine mutation in tyrosinase is responsible for the classical albino mutation in laboratory mice. Nucleic Acids Res *18*, 7293–7298.

Yu, F., Jiao, S., Lai, W., Liu, Z., Zhu, M., Zhu, W., Bai, C., Zhang, Y., Zhang, J., and Yan, S. (2018). Conserved aspartate-to-glycine mutation in tyrosinase is associated with albino phenotype in domestic guinea pigs (Cavia porcellus). Anim Genet *49*, 354–355.

Zhang, W., Wang, H., Brandt, D.Y.C., Hu, B., Sheng, J., Wang, M., Luo, H., Guo, S., Sheng, B., Zeng, Q., et al. (2021). The genetic architecture of phenotypic diversity in the betta fish (Betta splendens). BioRxiv 2021.05.10.443352.

Zhang, Y., Hong, Q., Cao, C., Yang, L., Li, Y., Hai, T., Zhang, H., Zhou, Q., Sui, R., and Zhao, J. (2019). A novel porcine model reproduces human oculocutaneous albinism type II. Cell Discov *5*, 48.